UNIVERSITY OF CALIFORNIA, SAN DIEGO

**Adversarial Strength Estimation Using Simulated Reconnaissance
Data for Urban Combat Operations**

A thesis submitted in partial satisfaction of the
requirements for the degree Master of Science

in

Engineering Sciences (Mechanical Engineering)

by

Dharmesh C. Panchal

Committee in charge:

    Professor William M. McEneaney, Chair
    Professor Thomas R. Bewley
    Professor Miroslav Krstić

2007

The thesis of Dharmesh C. Panchal is approved:

_____

_____

_____
                                                          Chair

University of California, San Diego

2007

To my Grandmother,

Who provided me with her elderly wisdom.

To my Mom,

Who nurtured and guided me

through the right course in life.

To my Dad,

Who would always be there whenever I run into trouble.

And to my brother Shashi,

Who would be the life of the family when things are mundane.

TABLE OF CONTENTS

LIST OF FIGURES

LIST OF TABLES

ACKNOWLEDGEMENTS

ABSTRACT OF THE THESIS

Adversarial Strength Estimation Using Simulated Reconnaissance Data for Urban Combat Operations

by

Dharmesh C. Panchal

Master of Science in Engineering Sciences (Mechanical Engineering)

University of California San Diego, 2007

Professor William M. McEneaney, Chair

Developing a model of the force distributions of an adversary has become an urgent need for military personnel, particularly in today's urban environment. In this thesis, we present and discuss the estimation of the adversarial strength and location using UAV-reconnaissance data from a simulated terrain. We will apply a stochastic model to our estimator and compare our results to our true data. We implement our model, obtain an error bound for our estimator, present several examples of observation-based estimator in conjunction with an urban combat simulator, and analyze the effects that our input parameters have on our resulting estimator.

1

Introduction

In today's combat environment, military analysts and commanders are in great need of obtaining an accurate assessment of an adversary's strength and location. This assessment can be determined based on the data that is collected from various observations made through unmanned autonomous vehicles (UAV's) deployed in the field. For example, we must estimate the force distributions of the adversary in an urban setting. To do this, we must develop an algorithm that analyzes the observation-based data and generates an estimator, which can be tabulated and graphically represented by a command and control simulator. In this thesis, using several mathematical tools, we present this strength estimator and analyze it, through simulations, with the ground truth itself.

The forces that are driving the need for such an estimate are the observer and the observed. That is, through UAV observations, we have the ability to collect detailed data of a complex environment such as an urban terrain. Also, we must consider that the situation on the ground, due to its complex nature, continues to change. Despite this gathering capability, we must determine a robust method to reinterpret the data so that it may become operationationally useful.

During a reconnaissance mission, we will be taking several observations of the urban environment (e.g. the terrain, buildings, elevation, population, etc.). We must develop an algorithm to process these observations in a computationally fast manner into viable data. In this thesis, we will focus on discrete observations based on adversarial manpower and try to reinterpret that information through our mathematical algorithm.

Like a Kalman filter, this algorithm will seek to objectively provide us with an estimate called *strength distribution*. At each time-step, we will have both observation

update and dynamic update, which corresponds to the potential movement of the adversarial forces. In the end, our goal is to generate a robustly accurate assessment of the adversary's state from information that tends to be subjective in nature.

1.1   List of Symbols

- $\mathcal{L}$: Set of all nodes on the graph.

- L: Total number of locations on the graph.

- N: Total possible strength for Red units.

- S_t: Strength distribution of Red units at time t.

- l: Main subset of all nodes of strength distribution, S_t.

- λ: Subset of nodes that are not part of l.

- $[S_t]_l$: Estimated Strength at location l at time t.

- H_t: True strength of Red units at time t.

- $[H_t]_l$: True Strength at location l at time t.

- $\mathcal{F}$: Matrix for dynamic flow update of Red units.

- $[y_t]_l$: The observed strength at location l at time t.

- I: Total number of iterations ran through Monte Carlo method.

1.2   Region of Interest

In this thesis, we choose a complex region in order to appropriately simulate the urban environment. In Figure 1.1, we see this complexity based on the description of the legend and the plot itself. We have approximately 9000 nodes/locations, which we refer to as waypoints (denoted by the black colored dots). These nodes are connected by edges. In the graph, we have several Blue and Red fire teams (denoted by asterisks) composed of multiple units. Each of these teams move can along adjacent location/nodes, connected by the edges. Some of these waypoints are stacked in this 2-D snapshot (e.g. the waypoints inside a multi-story building). Besides the waypoints and the Blue and
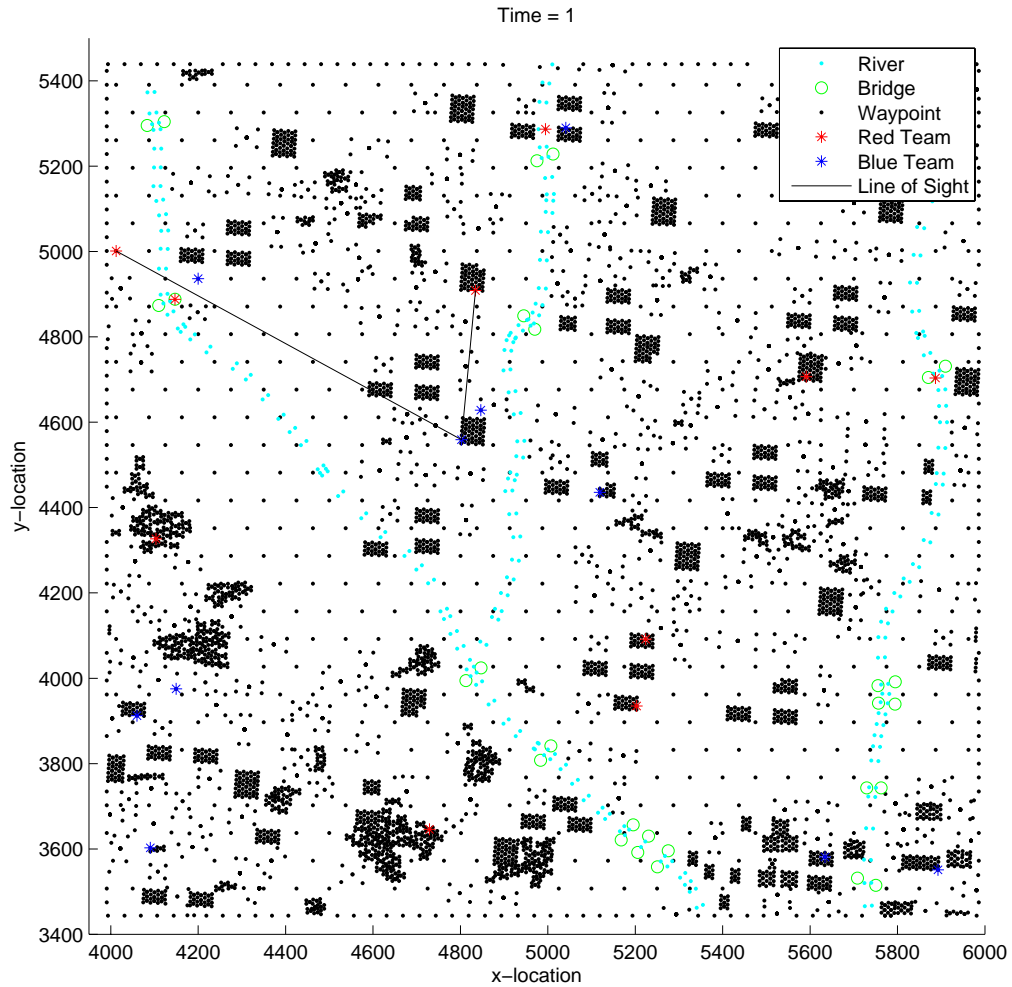
Figure 1.1: Region of Interest

Red teams, we have nodes that denote rivers and bridges in our graph. A team can only cross a river through a bridge. The solid lines between the Red and Blue teams indicate a line of sight occuring, which we will discuss later.

1.3   Strength Distribution

The state of the system of the urban environment would be the location and strength of the forces. The system will be composed of two types of forces: Red units and Blue units. Each unit may represent some firing team, with an associated strength, in the given terrain.

In Figure 1.1, we provided a plot of a large urban environment. Due to the complexity of the region (e.g. several thousand waypoints), we find it was best to implement our model within a subregion of the larger terrain. Due to sufficient number of waypoints, the presence of buildings, and lack of rivers, the arbitrary subregion we choose to focus on is the bottom left corner from the figure. Therefore, for the rest of this thesis, we will focus on the subregion displayed in Figure 1.2.

In Figure 1.2 below, we represent each of four Red teams and each of the four Blue teams by the different symbols of a circle, square, asterisk, and plus sign. The strength of the unit can be interpreted as manpower of the unit at a particular location. Since we are interested in estimating the strength and location of the adversary, we will primarily focus on the Red units, which represent as the adversary.
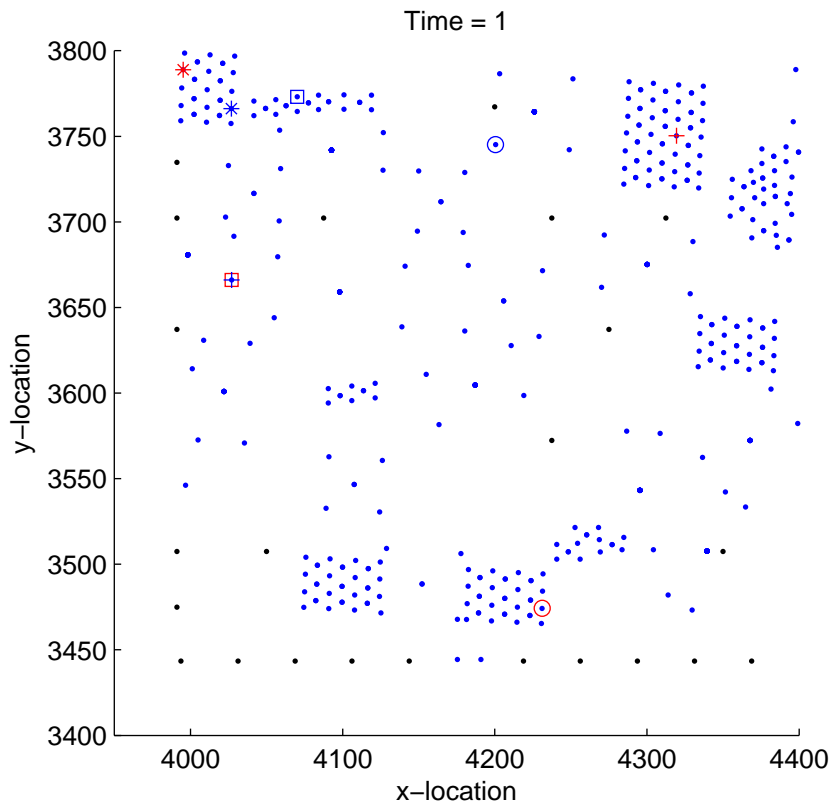
Figure 1.2: Sample Graph of Subregion

For the model that we discuss in this thesis, we will focus within the subregion and analyze how our estimate compares with our true data. For most of our simulations, we will observe the behaviors of one Red team represented by circles(s) on the graph

and determine how well our estimate matches with the truth of that Red team. In our subregion, we will have approximately $L = 500$ locations/nodes in which the Red team will move across on the graph. We will observe two cases: the deterministic and the stochastic cases.

For the strength distribution, we define the estimated strength S_t as a two-column nodal set. At each time-step t, the first column represents the nodal location and the second column represents the nodal strength of the adversary for the corresponding location.

1.4 Observation Update

We may have multiple observations occurring at a given time-step t. We represent these observations as an order pair (l, y) where l denotes the location of observation in $\mathcal{L}$ and y is the observed strength at node l. They are both integers where $l \in \mathcal{L}$ and $y \in Z^+$, since we only observe discrete units.

We motivate our estimator form construction with standard Bayesian propagation. Suppose that prior to the observation, the probability that a Red unit is at l is denoted by P_l. Also, suppose that one observes the unit at node z. Let $P(z|\lambda)$ denoted the probability that one observes unit at z given that it is at node λ. By applying Bayesian propagation, the a posteriori probability distribution [1, 2, 3] is

$$\hat{P}_l = \frac{P(z|l)}{P(z|l)P_l + \sum_{\lambda \neq l} P(z|\lambda)P_\lambda} P_l,$$

and also, for $\lambda \neq l$,

$$\hat{P}_\lambda = \frac{P(z|\lambda)}{P(z|l)P_l + \sum_{\lambda \neq l} P(z|\lambda)P_\lambda} P_\lambda.$$

We use the above Bayesian propagation to derive the following form of our strength update. Given a priori (pre-observation) strength S_t, the a posteriori (post-observation) strength, $\widehat{S}_t$, is determine by the following equation [1, 2, 3]:

$$[\widehat{S}_t]_l = \frac{1 + \delta}{1 + \frac{\delta [S_t]_l}{N}} [S_t]_l \tag{1.1}$$

$$[\widehat{S}_t]_\lambda = \frac{1}{1 + \frac{\delta [S_t]_l}{N}} [S_t]_\lambda \quad \forall \, \lambda \neq l, \tag{1.2}$$

where $\delta = \delta(y, [S_t]_l)$.

We define δ so that we obtain an estimate, $[S_t]_l$, that converges to our observation, y. We therefore choose $\delta = \delta(y, [S_t]_l)$ to be

$$\delta(y, s) = k \left[\frac{y - s}{s} \right], \tag{1.3}$$

where $k \in (0, 1)$. Our selection of k will depend on level of confidence in our observation, y.

When we apply an observation update to a given location, we state that the total strength within our strength distribution is conserved. We show this in Proposition 1.4.1[1, 2, 3]:

Proposition 1.4.1 *Suppose* $\sum_{l \in \mathcal{L}} [S_t]_l = N$. *Then,* $\sum_{l \in \mathcal{L}} [\widehat{S}_t]_l = N$.

PROOF. Noting that $\sum_{\lambda \neq l} [S_t]_\lambda = N - [S_t]_l$, one has

$$\begin{aligned}
\sum_{k \in \mathcal{L}} [\widehat{S}_t]_k &= \sum_{\lambda \in \mathcal{L} \setminus \{l\}} [\widehat{S}_t]_\lambda + [\widehat{S}_t]_l \\
&= \frac{N - [S_t]_l}{1 + \frac{\delta[S_t]_l}{N}} + \frac{1 + \delta}{1 + \frac{\delta[S_t]_l}{N}} [S_t]_l = N.
\end{aligned}$$

Through our selection of δ, we redefine the observation update by the following equations:

$$[\widehat{S}_t]_l = G(y, [S_t]_l) \tag{1.4}$$

$$[\widehat{S}_t]_\lambda = F(y, [S_t]_l)[S_t]_\lambda \tag{1.5}$$

where

$$G(y, s) = \frac{1 + k \left(\frac{y-s}{s} \right)}{1 + k \left(\frac{y-s}{N} \right)} s = \frac{s + ky - ks}{1 + \frac{ky - ks}{N}} \tag{1.6}$$

$$F(y, s) = \frac{1}{1 + k \left(\frac{y-s}{N} \right)}. \tag{1.7}$$

In our simulations, we model the observations of the Red units through different means. This depends on whether we want measurements using deterministic data or random observations. The deterministic data is based on terrain constraints: whether there is line-of-sight (LOS) between the Red unit location and the given location of the Blue units. We must also consider that we may have noise in our observations.

On the other hand, we can generate observations randomly. We use the parameter, p_l, which is the probability of observing a unit at l.

1.5   Dynamics Update: Strength Flow

We assume that the dynamics in the system are represented by the movement of the Red units. The movement itself would have possible observed and unobserved inputs at each time-step. We model the movement dynamics as a Markov Model. For instance, a set of Red units with estimated strength distribution [1, 2, 3, 4] of S_t at time t would have a distribution at the next time-step given by

$$S_{t+1} = \mathcal{F}^T S_t, \tag{1.8}$$

where $\mathcal{F}$ is $L \times L$ transition matrix of the Red units. In our application, we will model this motion through two means: deterministic and stochastic motion.

For the deterministic motion, we assume that there is natural definite flow of Red units on the nodal graph, where each of the adjacent nodes is still connected by edges. The units will flow on the graph based on data that is provided to us with regards to the terrain (e.g. Red units move on shortest path).

For stochastic motion, we model the motion of the Red units differently. Instead, we are focused on the probable location of the Red units. The Red units will flow by equation 1.8, but the graph for stochastic motion will present the probable location and strength of our estimate. Given that the diagonal entries of our flow matrix, $0 < \mathcal{F}_{i,i} < 1$, we know that our resulting estimate at each time-step is due to a Markovian motion.

1.6   Thesis Content, Objectives, and Analysis

The primary purpose for this document is to present the application of the strength estimator through simulations that use the proposed estimator form. Through these means, we are able to verify whether these tools hold true or not. We will implement the concepts discussed in this introduction in Command and Control simulator to understand how they work. If our estimator reflects the ground truth, then we know they work as predicted.

In our main content, we will apply the stochastic tools by conducting several simulations and compare our obtained strength estimator with the ground truth data. This data depends upon the knowledge we have of the Red units. That includes the location of the units, their movements, and their strength. Ultimately, the implementa-

tion of these tools will determine how well our estimate will be, compared to the ground truth itself.

Finally, once we have completed our simulations, we will analyze and discuss how well our estimator, S_t, compares with the ground truth. In this thesis, we will primarily analyze the case where we have stochastic motion of the Red units. That is, we have imperfect knowledge of the true movement of the Red units and, instead, only have an idea of the probable locations of movement. We analyze the relationship between our input parameters and our resultant estimator by computing of the error and standard deviation between our estimator and the true strength at each input parameter in our model.

2

Application of Estimator Using Offline Data

We now provide details on the implementation on the proposed estimator via a simulation example. We determine how well our estimator will match up with prerecorded offline data gathered from a ground UAV for a given terrain. In this chapter, we will discuss the implementation of the flow dynamic update and the observation update using offline ground truth data of the terrain itself. From this data, we will produce an estimated strength distribution of the adversary at each time-step.

2.1   Simulation Example: Flow and Observation Update Using Offline Data

In the following simulation, we use the offline data to produce an estimator of the ground truth. We assume that we do not have aerial UAV capability and must rely on Blue teams on the ground to conduct reconnaissance. For one of the data that we apply, we use the actual ground truth movement of the Red and Blue teams in our ground truth. These teams move along the shortest path in the given terrain that is predetermined using the data provided. In our simulation, we denote the paths of the Red and Blue teams with lines that correspond to there color. We choose to have five Red teams and five Blue teams that start at arbitrary locations within our graph so that we may encounter frequent observations of the Red units. These observations of the Red teams by the Blue teams occur when we have a line of sight (LOS) between

two waypoints. We predetermined this line of sight from the data provided to us. Since, realistically, we do not always have perfect observation of the adversary, our observation measurements can vary and do not necessarily have to match the truth. In this example, our measurements are denoted by a natural number y such that $0 \leq y \leq 6$ and we choose $k = 0.95$. Using these measurements, we update our strength estimator using the observation update discussed in the introduction. Thus, as one will see, for example, on the left plot in Figure 2.1, the Red and Blue teams will move within the graph with the Blue team taking an observation of the Red team when appropriate.
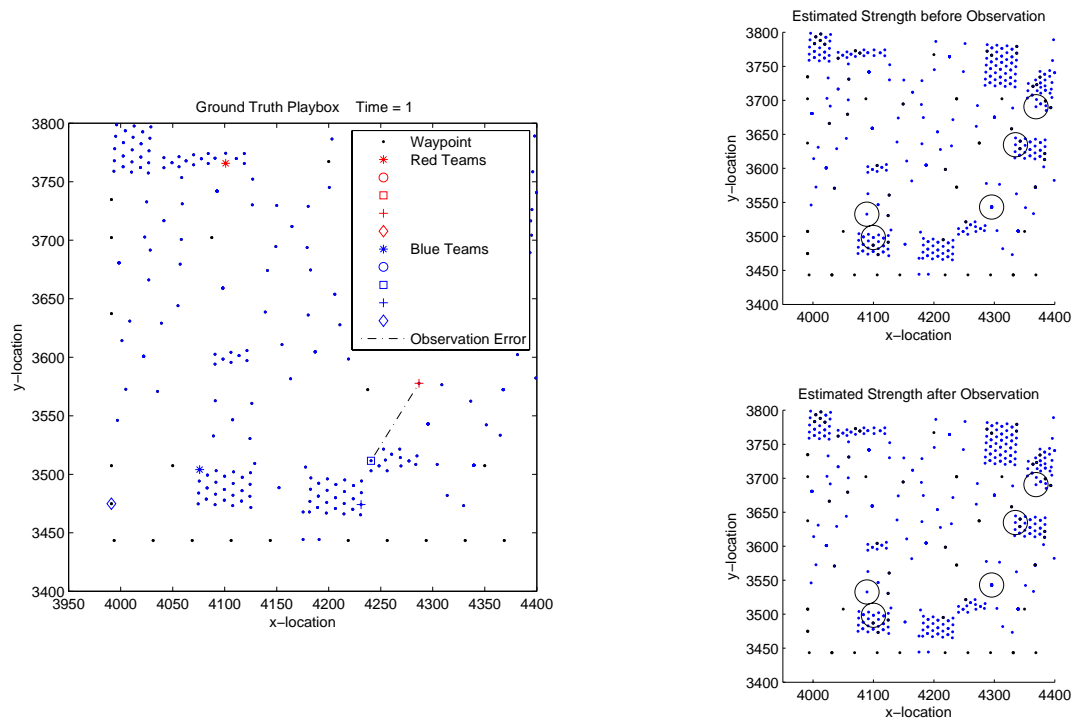
Figure 2.1: Movement and Obserevation Snapshot, Time-Step 1

In our figures, we denote each of the Red and Blue teams with a unique symbol (i.e., asterisk, circle, diamond, square, and plus sign). For our strength estimator, we choose to focus on 50 arbitrary locations out of the 500 locations for our l subset. The rest will make up the λ subset. We will set the the total strength of all the Red teams combined to be $N = 15$. Whenever we have a LOS between Blue and Red teams, we denote in our graph with a solid black line between the Red and Blue teams.

However, we may also have errors in our observation. As a result, the Blue team

may not see the Red team even though we have a LOS. We denote this "missed"observation as shown in Figure 2.1 by a dash-dotted black line displayed between the Red and Blue teams. We may encounter this instance whenever we compare a random variable with a tolerance in the algorithm for our simulation. We compute this tolerance by measuring the distance between the two teams. We divide this distance with the maximum possible distance in graph itself.

Besides an algorithm to produce the ground truth in our simulation, we also apply flow dynamic update and the observation update to produce the estimated strength distribution in our simulation. In our ground truth graph, whether we have an observation or not, we still run a flow dynamic update in our simulation. In this simulation, we take the main diagonal of our transition matrix, $\mathcal{F}$, to be $\mathcal{F}_{i,i} = \eta = 0.5$, which means that half of the strength mass at a particular location in our strength estimator will stay at the current location while the other half will redistribute equally to all nearby connected locations. Taking the observation data from our graph, we compute an observation update in our algorithm corresponding to the location of observation, thus updating our estimated strength distribution. For each time-step, we represent this distribution in our simulation with the two right-half plots in Figure 2.1. We show the a priori and a posteriori observations in the two plots.

In the two right-half plots, we denote the strength distribution by the various sizes of the black circles on the graph. We make an initial conjecture of where our strength distribution, S_t, will be concentrated as shown by the top right plot in the figure. Since we have five Red teams and the total strength is $N = 15$, we will initially surmise that each of the teams has a true strength of 3. Our distribution will change at each time-step based on the changes in our ground truth as well as our flow and observation update. Whenever we have a LOS between the Blue and Red teams, we have an observation in the strength distribution plots. We denote the observation by either a magenta or red circle. Whenever we obtain an observation within the l subset, we denote that by the red circle. If the observation occurs outside the set, we denote it by the magenta circle.

2.1.1 Continuation of the Simulation from Previous Section

In the ground truth plot in Figure 2.1, we would generally have an observation based on the LOS between a Red and Blue teams. However, according to the dashed-

dotted line, we have an observation error occurring between the two opposing teams. As a result, we have no observation update at the very first time-step, and, therefore, our a priori and a posteriori observation plots remain the same. The only update that we consistently have at each time-step is the dynamic flow update, which we see occurring in the two right-half plots. We notice that in addition to our initial "guess"(large black circles in the plot), we also have smaller circles that were distributed from the large circles through the dynamic flow update in our algorithm.
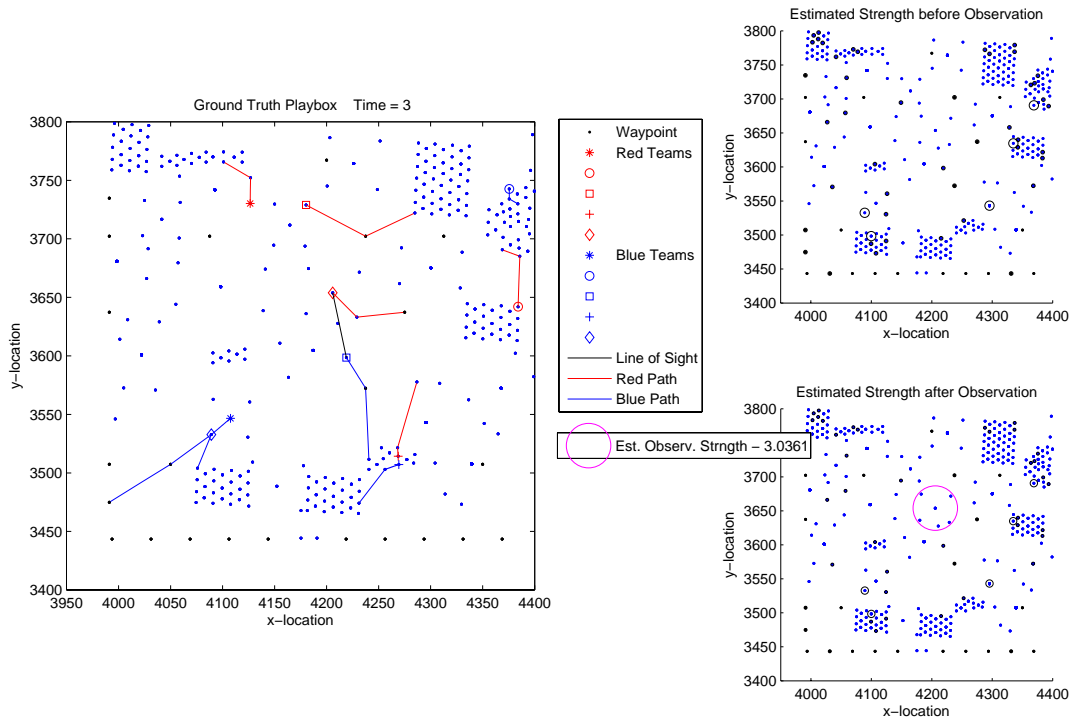
Figure 2.2: Movement and Observation Snapshot, Time-Step 3

As we increase the time-steps in our simulation, we see both the Red and Blue teams moving along their shortest path in the ground truth plot. We have our first LOS in Figure 2.2 between a Blue and Red team. As a result of that LOS, we have an observation that occurs outside the l subset. This "new"location will become part of the l subset, while one of the locations with negligible strength is disregarded. The large magenta circle indicates that, at that location ($S_l = 3.0361$), we have an overestimated measurement observation. That is, our measurement y was greater than our initial conjecture of each of the Red teams. We note that our estimate is $S_l = 3.0361$ and not

$S_l = 3$. We clearly have an imperfect observation on the ground truth. As a result, our observation update is computationally designed so that our estimate, S_l, converges to y and not necessarily $S_l = y$.

In addition, the other circles in our distribution have reduced in size. Since the strength mass is conserved, the total strength in our distribution will not change ($N = 15$). This means that some of the the mass from our initial conjecture is redistributed to our newly observed location.
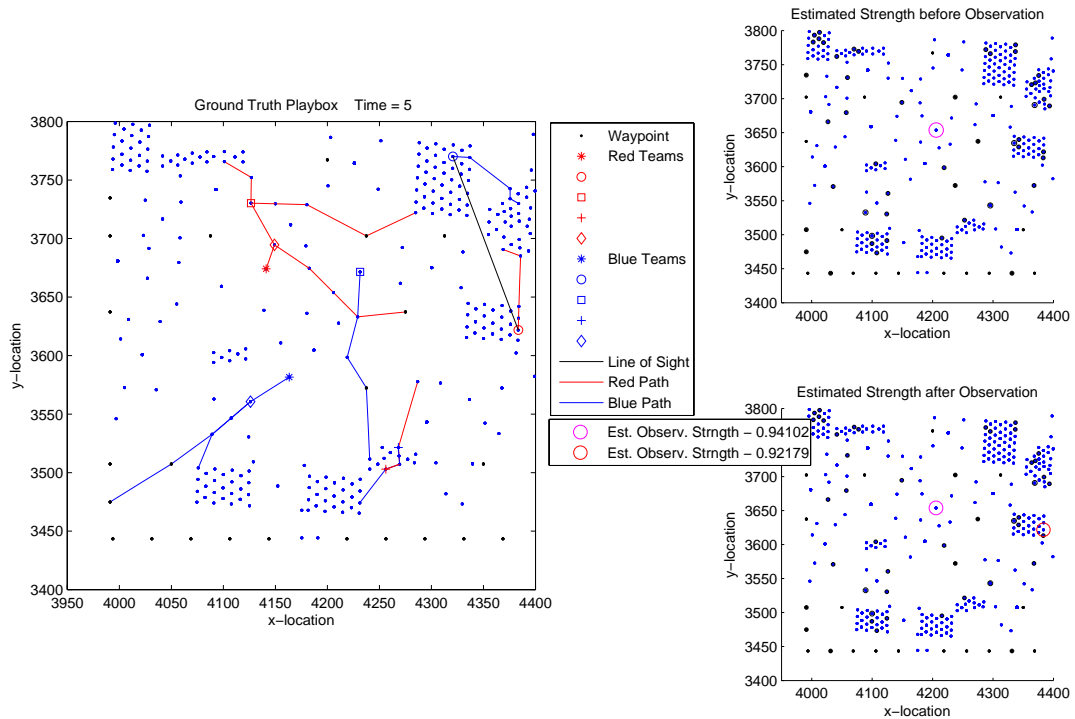
Figure 2.3: Movement and Observation Snapshot, Time-Step 5

In our final time-step, we have an observation occurring inside the l subset as indicated by the red circle in the a posteriori plot in Figure 2.3. Also, if we note the size of the red circle, we see that the estimated observed strength is relatively small ($S_l = 0.92179$) compared to the observation that we had during our previous time-step. This indicates that our measurement y was underestimated from our initial conjecture. Also, if we look at the previous observation, we notice that it has reduced greatly from its original size ($S_l = 0.94102$). This is the direct consequence of our flow update and observation update, where much of that strength mass has been redistributed throughout the graph.

Generally, in this simulation, we continue to update our strength distribution whenever we have an observation update. This means that the more observations that we have of the Red units at each time-step, the more accurate our estimator will be. The location of the Red teams continue to change in our graph, and they are not moving through stochastic motion but along a fixed shortest path. Since our observation measurements depend upon fixed LOS data between the Blue and Red teams on the ground and the movement of the Red teams is fixed, our estimate may not accurately reflect the state of the adversary. In this case, this simulation suggests that modeling the truth itself using the stochastic tools presented can have limited effectiveness. That is, the appropriate use of the tools would depend upon the initial knowledge we have of the Red units and knowledge that we gain at each incremental time-step.

3

Deterministic Movement

We look at the deterministic movement in order to develop an better idea in regards how effective our methods will be assuming that we have perfect knowledge of the terrain itself and the troop's actual movements. In the deterministic movement, we maintain a fixed nominal path for which the Red units move on the given terrain. We, from there, compare this ground truth to the estimator itself. Suppose that the Red units were to diverge from the nominal path. We therefore must update our estimator to take this into account. This is where the observation update allows us to improve our estimate.

3.1   Movement Dynamics

For deterministic movement, we assume that there is a natural flow of Red units on the graph composed of a set of nodes, $\mathcal{L}$, called waypoints, which are connected through edges. These edges are represented by an $L \times L$ symmetric matrix, $\mathcal{F}$ where $\mathcal{F}_{i,j}$ is one if nodes i and j are adjacent or zero otherwise. In the deterministic movement, the flow matrix may have each row with a single entry of one and the remaining entries being zero. For example, for each $l \in \mathcal{L}$, we have $k \in \mathcal{L}$ such that $\mathcal{F}_{l,k} = 1$ and $\mathcal{F}_{l,\lambda} = 0$ for all $\lambda \neq k$. This matrix construction helps define where Red units nominally move from node l to node k. Therefore, given the true strength distribution H_t at time t, the true strength distribution at the next time-step is given by

$$H_{t+1} = \mathcal{F}^T H_t. \tag{3.1}$$

Suppose now the Red commander inputs a control signal changing the move-

15

ment of the Red units. We will represent this control input by an $L \times L$ symmetric matrix, U_t, which modifies the nominal movement given by $\mathcal{F}$. The modification of, say node $l \in \mathcal{L}$, occurs through the elements of the lth row of U_t. If there is no control input at node l at time t, then the lth row of U_t will compose of entirely of zeros.

For example, suppose the Red commander inputs a signal to change the Red units movement from node l. The flow matrix, $\mathcal{F}$, remains unchanged. The nominal movement from node l to k, as stated in the beginning paragraph, is represented by the entry, $\mathcal{F}_{l,k} = 1$. One of the entries for the control matrix, U_t, will be $[U_t]_{l,k} = -1$, where k is the same index referring to the destination node k in the flow matrix, $\mathcal{F}$. We denote the revised destination node as κ. Therefore, the other significant entry is $[U_t]_{l,\kappa} = 1$. All of the remaining entries of the lth row of U_t will be zeros. To clarify this, we provide a matrix example of our flow and commander input matrices:

$$
\mathcal{F} = \begin{pmatrix} 0 & 1 & 0 & \dots & 0 \\ 1 & 0 & 0 & \dots & 0 \\ 0 & 0 & 0 & \dots & 1 \\ \cdot & \cdot & \cdot & \cdot & \cdot \\ 0 & 0 & 1 & \dots & 0 \end{pmatrix}, \ U_t = \begin{pmatrix} 0 & -1 & 0 & \dots & 1 \\ 0 & 0 & 0 & \dots & 0 \\ 0 & 0 & 0 & \dots & 0 \\ \cdot & \cdot & \cdot & \cdot & \cdot \\ 1 & 0 & -1 & \dots & 0 \end{pmatrix} \tag{3.2}
$$

$$
\mathcal{F} + U_t = \begin{pmatrix} 0 & 0 & 0 & \dots & 1 \\ 1 & 0 & 0 & \dots & 0 \\ 0 & 0 & 0 & \dots & 1 \\ \cdot & \cdot & \cdot & \cdot & \cdot \\ 1 & 0 & 0 & \dots & 0 \end{pmatrix}. \tag{3.3}
$$

If we compare our example nominal flow matrix, $\mathcal{F}$, with Matrix 3.3, $[\mathcal{F} + U_t]$, we see that have at least two commander inputs from the first and L^{th} row of the matrix. Thus, the true strength distribution [3] with the commander input is given by

$$
H_{t+1} = [\mathcal{F} + U_t]^T H_t \tag{3.4}
$$

If there are no commander inputs in our deterministic model, we simply take $U_t \equiv 0$. Also, the dynamic flow update remains unchanged for the estimated strength. That is, the strength distribution is given by

$$
S_{t+1} = \mathcal{F}^T S_t. \tag{3.5}
$$

Notice that if there is a commander input, the estimated strength still flows nominally.

In addition to the dynamic flow update for the estimated strength, we also include observation update for the estimated strength that occurs based on observation measurements taken from the true strength. We take these observations randomly using the observation update defined in the introduction and we assume that our observations are imperfect. For each subset $l \in \mathcal{L}$ and $\lambda \in \mathcal{L} \setminus \{l\}$, the observations in our simulations are respectively given by the equations:

$$\widehat{S}_l = \frac{S_l + ky - kS_l}{1 + \frac{ky - kS_l}{N}} \tag{3.6}$$

$$\widehat{S}_\lambda = \frac{1}{1 + k\left(\frac{y - S_l}{N}\right)} S_\lambda. \tag{3.7}$$

3.1.1 Input to Output Error Bounds

To further understand the extent our strength estimator converges or diverges from the ground truth as a result of the commander input, we will examine the error bounds for the flow dynamics. We will apply Theorem 3.1.3 to see this. Since we compare our estimator, S, to our ground truth, H, we must choose a bounds that reflects this. We therefore bound the **L1** norm (also called Least Absolute Deviations) of the estimator error as a function of **L1** norm of the deterministic components of the system. Also, for an $L \times L$ matrix, M, we apply $|M|$ to denote the induced norm on the matrix as a linear operator. That is, $|M| = \sup_{|s| \le 1} |Ms|$.

Remark 3.1.1 [3] It is well-known that the induced norm of the transpose of a stochastic matrix (i.e., a square matrix satisfying (4.1)) is one. To see this, note that

$$|M^T s| = \sum_{\lambda=1}^{L} \left| [M^T s]_\lambda \right| = \sum_{\lambda=1}^{L} \left[\sum_{l=1}^{L} M_{l,\lambda} |s_l| \right]$$

$$= \sum_{l=1}^{L} \left[\sum_{\lambda=1}^{L} M_{l,\lambda} \right] |s_l| = \sum_{l=1}^{L} |s_l| = |s|.$$

Lemma 3.1.2

$$|S_{t+1} - H_{t+1}| \le |S_t - H_t| + |U_t||H_t| \le |S_t - H_t| + N|U_t|. \tag{3.8}$$

As one may recall from above, we define the dynamics of the deterministic case for the true strength as

$$H_{t+1} = [\mathcal{F} + U_t]^T H_t, \tag{3.9}$$

while the dynamics for the estimated strength is

$$S_{t+1} = \mathcal{F}^T S_t. \tag{3.10}$$

PROOF.   From (3.9) and (3.10),

$$
\begin{aligned}
|S_{t+1} - H_{t+1}| &= \left| \mathcal{F}^T S_t - \left(\mathcal{F}^T + U_t^T \right) H_t \right| \\
&\leq \left| \mathcal{F}^T (S_t - H_t) \right| + \left| U_t^T H_t \right| \\
&\leq |S_t - H_t| + |U_t^T| \, |H_t| \, .
\end{aligned}
$$

Theorem 3.1.3 *[3] Let the true strength dynamics update be given by (3.9) in the deterministic case. Let the strength estimator update be given by (3.10). Then, in the deterministic, we have*

$$|S_t - H_t| \;\; \leq |S_0 - H_0| + N \sum_{r=0}^{t-1} |U_r^T|$$

for all $t \geq 0$, respectively.

PROOF.   The proof is immediate by Lemma 3.1.2 and an induction argument.

3.2   Simulation Example: True Strength versus Estimated Strength

For simplicity of exposition, we choose to have only one Red team on a graph of approximately 500 locations/waypoints. We run the simulation for five time-steps in order to compare the long term differences between the strength estimator and the true strength. In our simulation, we focus on a small region from a larger area of interest. The color coding in the larger area depicts the terrain type of the location, i.e., water bodies, building corners, etc. The Red team starts at the same location at the beginning of the simulation regardless of whether we have a commander input. We designate the Red team with a true strength of $H_l = 3$. In our simulation figures for the true strength plot, we display the actual position (the red circle) of the Red team, which includes the commander input, as well as nominal position (the green diamond) of the Red team. In addition, we trace the path of the Red teams actual path and nominal path using their corresponding color.

For the simulation of the estimated strength, we represent the Red team as black circle(s) that move nominally. We have a random observation that occurs in our simulation such that our observation parameter is $p_l = 0.5$. Whenever an observation occurs, the black circle(s) break off into smaller circles where the magenta circle represents the location of the observation that corresponded to the actual Red team position. We choose $k = 0.95$ in the observation update. For each time we run the simulation, the final distribution of the true strength, H_t, remains unchanged, while the final distribution for the estimated strength, S_t, can vary.

In addition, we compute the error bound given by Theorem 3.1.3 at each time step. We compare the left side and the right side of the inequality.

3.3   Simulation Results
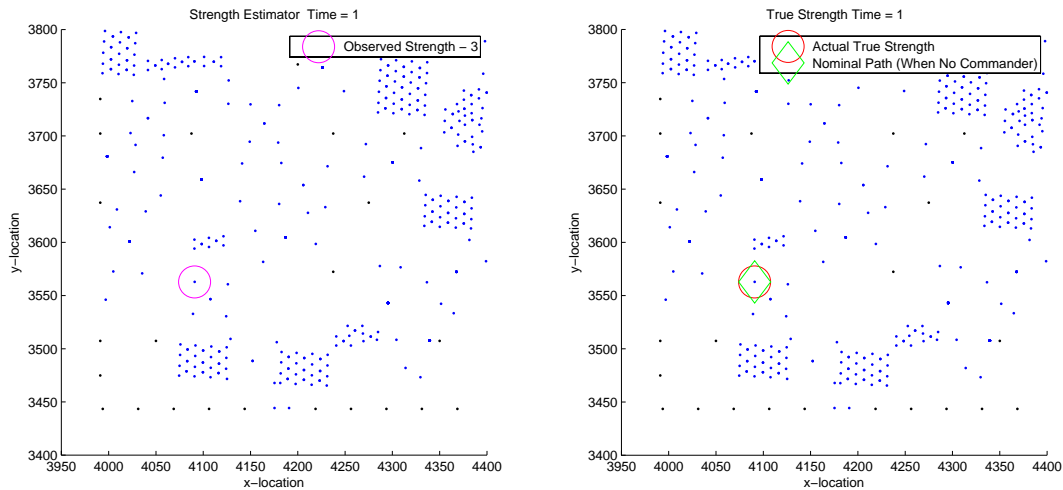
Figure 3.1: Deterministic Movement, Initial Time-Step

In Figure 3.1 on the right-half side, we have the Red team's actual position starting at the same place as the nominal position. We also note that for each time-step, the Red team does not remain idle at the same place. That is, mathematically, the flow matrix for the deterministic case, $\mathcal{F}$, has its main diagonal entries, $\mathcal{F}_{i,i} = 0$. The strength estimator on the left side also starts at the same nominal location as on the right side. Notice that the color of the circle is magenta, indicating that Red team is observed at that starting location.
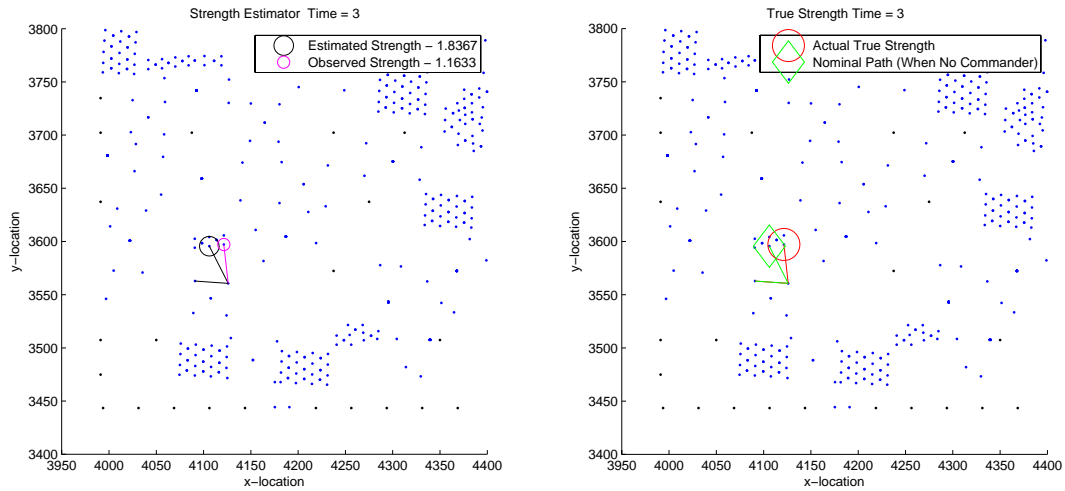
Figure 3.2: Deterministic Movement, Time-Step 3

In Figure 3.2, we see on the right-half plot that the actual location diverges from the nominal location. This clearly indicates that the Red team received a command input to move to a different location. As a result of this divergence, the original larger circle in our estimated strength plot (left-half plot) breaks off into two smaller circles: one representing where the observation occurred (magenta), the other continuing to move along the nominal path (black).
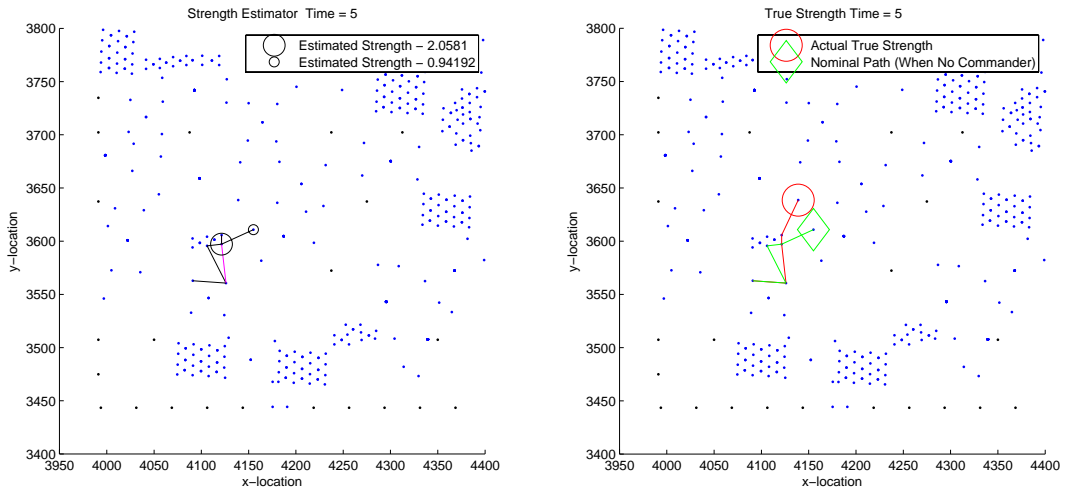
Figure 3.3: Deterministic Movement, Final Time-Step

At the final time-step, the Red team receives another commander input, thus diverging from the nominal location. For the estimated strength plot (left side), however, since we do not have an observation taken of the Red team, the final movement for the estimator is nominal.

3.3.1 Analysis: Dynamics Effects

Table 3.1: Dynamic Error Bounds

Time-steps	Left Side	Right Side
1	0	0
2	0	0
3	3.6735	6
4	3.0769	12
5	6.0000	18

We computed and tabulated the error bounds (See Table 3.1) from our simulated data to verify if they were consistent with Theorem 3.1.3. We bound the estimation errors by a function of the **L1** norm. We do not see any changes to our error bounds until the third time step. Recall we had a commander input at that step, therefore leading our Red troops away from the nominal path. Since we do not have perfect observation of the Red troops, we have a bound that is greater than zero. The larger the left side is, the larger the measurement of our error will be. The right side indicates how frequently we had a commander input. As the right side increases at each time-step, then by Theorem 3.1.3, we see an increase in commander inputs. In Table 3.1, we had three commander inputs total in our simulation.

4

Stochastic Flow

We need to use a robust model that provides us with the best assessment of the adversarial location and strength. Since we may never have perfect knowledge of the terrain, the movement of the Red units, and the conditions on the ground, we therefore must consider a stochastic model as our estimator. The stochastic model provides us with an estimate, S_t, composed of the most probable location and strength of an adversary. We update this estimate through various stochastic concepts such as Markov chains, Bayes' rule, and normal distributions.

4.1 Movement Dynamics

For the stochastic movement, we model the motion of Red units in the form of a Markov chain. Like deterministic motion, we still have a graph composed of nodes (or waypoints) that are connected by edges. These edges are still represented by an $L \times L$ symmetric matrix, $\mathcal{F}$. However, in stochastic motion, each row will have entries that are less than one or equal to zero. For example, for each node $l \in \mathcal{L}$, we have connected nodes $k \in \mathcal{L}$ such that $\eta_{nom} = \mathcal{F}_{l,l} = 0.9$, $\mathcal{F}_{l,k}$ corresponds to the connected nodes where the remaining mass is evenly distributed, and $\mathcal{F}_{l,\lambda} = 0$ for all $\lambda \neq k$. Like a true Markov property, the sum of each row will equal one. More specifically, we state that the flow matrix, $\mathcal{F}$, has the property [3, 4] such that

$$\mathcal{F}_{i,j} \in [0,1] \quad \forall\, i,j \in \mathcal{L}, \text{ and } \sum_{j \in \mathcal{L}} \mathcal{F}_{i,j} = 1 \quad \forall\, i \in \mathcal{L}. \tag{4.1}$$

We are essentially defining the nominal movement through this matrix construction where we try to determine the most probable movement of the Red units. By

defining the flow matrix in this manner, the expected true strength distribution of the Red units for each time-step is given by

$$\mathbf{E}[H_{t+1}] = \mathcal{F}^T \mathbf{E}[H_t]. \tag{4.2}$$

Suppose now the Red commander inputs the control signal to change the probable flow of the Red units. Like the deterministic case, we will still represent this control input by an $L \times L$ symmetric matrix, U_t, which modifies the nominal flow given by $\mathcal{F}$. This modification of, say node $l \in \mathcal{L}$, occurs through the elements of the lth row of U_t. The modification does not, however, change the basic Markov property of the overall flow matrix. That is, we set the constraint for U_t to be

$$[\mathcal{F}]_{i,j} + [U_t]_{i,j} \in [0, 1] \quad \forall\, i, j \in \mathcal{L}$$
$$\sum_{j \in \mathcal{L}} [\mathcal{F}]_{i,j} + [U_t]_{i,j} = 1 \quad \forall\, i \in \mathcal{L}.$$

As before, if there is no control input at node l at time t, then the lth row of U_t will compose of entirely of zeros.

For example, suppose the Red commander inputs a signal to change the Red units flow from node l. The flow transition matrix, $\mathcal{F}$, remains unchanged. The nominal flow from node l to k, as stated in the beginning, is represented by the entries, $\eta_{nom} = \mathcal{F}_{l,l} = 0.9$ and $\mathcal{F}_{l,k}$ represents the nearby connected nodes where the remaining strength mass distributes. Now suppose we wish to modify the flow at node l so that the actual flow is given by $\eta_{com} = 0.4$. Therefore, the diagonal entry for the control matrix, U_t, will be the difference between 0.4 and $\mathcal{F}_{l,l} = 0.9$, $[U_t]_{l,l} = -0.5$. The entries, $[U_t]_{l,k}$, are determined through similar means. All of the remaining entries of the lth row of U_t will be zeros. Thus, the expected true strength distribution with the commander input [3] is given by

$$\mathbf{E}[H_{t+1}] = [\mathcal{F} + U_t]^T \mathbf{E}[H_t]. \tag{4.3}$$

If there are no commander inputs in our stochastic model, we simply take $U_t \equiv 0$. Also, the dynamic flow update remains unchanged for the estimated strength. That is, the strength distribution is given by

$$S_{t+1} = \mathcal{F}^T S_t. \tag{4.4}$$

Therefore, we still have nominal flow for stochastic motion.

Also, once a flow dynamic update takes place for the estimated strength, we leave the probability that an observation update takes place at a particular time-step. Now, assuming that we have noise in our stochastic model, we take observations randomly using the same observation update:

$$\widehat{S}_l = \frac{S_l + ky - kS_l}{1 + \frac{ky - kS_l}{N}} \qquad (4.5)$$

$$\widehat{S}_\lambda = \frac{1}{1 + k\left(\frac{y - S_l}{N}\right)} S_\lambda. \qquad (4.6)$$

4.2   Input to Output Error Bounds

4.2.1   Dynamics Only

We bound **L1** norm of the estimator error as a function of **L1** norm (also know as Least Absolute Deviations) of the deterministic components of the system. Like the deterministic case, we choose the **L1** norm because we want to compare our estimator, S_t, to our expected ground truth, $\mathbf{E}[H_t]$.

Lemma 4.2.1 *[3]*

$$|S_{t+1} - \mathbf{E}[H_{t+1}]| \le |S_t - \mathbf{E}[H_t]| + |U_t||\mathbf{E}[H_t]| \le |S_t - \mathbf{E}[H_t]| + N|U_t|. \qquad (4.7)$$

As one may recall from Chapter 1, we define the dynamics of the stochastic case for the true strength as

$$\mathbf{E}[H_{t+1}] = [\mathcal{F} + U_t]^T \mathbf{E}[H_t], \qquad (4.8)$$

while the dynamics for the estimated strength is

$$S_{t+1} = \mathcal{F}^T S_t. \qquad (4.9)$$

PROOF.   From (4.8) and (4.9),

$$
\begin{aligned}
|S_{t+1} - \mathbf{E}[H_{t+1}]| &= \left|\mathcal{F}^T S_t - \left(\mathcal{F}^T + U_t^T\right)\mathbf{E}[H_t]\right| \\
&\le \left|\mathcal{F}^T (S_t - \mathbf{E}[H_t])\right| + \left|U_t^T \mathbf{E}[H_t]\right| \\
&\le |S_t - \mathbf{E}[H_t]| + |U_t^T| \, |\mathbf{E}[H_t]| \, . \square
\end{aligned}
$$

Theorem 4.2.2 *[3] Let the true strength dynamics update be given by (4.8) in the stochastic case. Let the strength estimator update be given by (4.9). Then, in the stochastic, we have*

$$|S_t - \mathbf{E}[H_t]| \ \le |S_0 - \mathbf{E}[H_0]| + N \sum_{r=0}^{t-1} |U_r^T|$$

for all $t \ge 0$, respectively.

PROOF.   The proof can easily be shown by Lemma 3.1.2 and an induction argument.

4.2.2   Dynamics with Observation Disturbance Effects

We, in addition, have error bounds for the observation. We obtain the a posteriori estimated strength error, given the a priori error. We will consider two separate cases for this error bound: $[H_t]_l \ge [S_t]_l$ and $[H_t]_l < [S_t]_l$. We will show the former case first.

For the simplicity of notation, we will drop the subscript t. We denote S_l to be $[S_t]_l$, $\widehat{S}_l$ to be $[\widehat{S}_t]_l$, and H_l to be $[H_t]_l$. First, we note that

$$\widehat{S}_l = \frac{S_l + k(y - S_l)}{1 + k\frac{(y - S_l)}{N}}. \tag{4.10}$$

Solving for y, we obtain

$$\overline{y} \doteq \overline{y}(\widehat{S}_l, S_l) \doteq \frac{\widehat{S}_l - S + kS(1 - \widehat{S}_l/N)}{k(1 - \widehat{S}_l/N)}. \tag{4.11}$$

By differentiating with respect to $\widehat{S}_l$, one finds that

$$\frac{\partial \overline{y}}{\partial \widehat{S}_l} = \frac{N(N - S_l)}{k(N - \widehat{S}_l)^2} > 0. \tag{4.12}$$

We find that $\overline{y}$ monotonically increases as a function of $\widehat{S}_l$. Therefore, for the following lemma, we define $y^u = \overline{y}(H_l, S_l)$. As a reminder, we define $G(y, S_l)$ and $F(y, S_l)$ as the following:

$$G(y, S_l) = \frac{S_l + ky - kS_l}{1 + \frac{ky - kS_l}{N}} \tag{4.13}$$

$$F(y, S_l) = \frac{1}{1 + k\left(\frac{y - S_l}{N}\right)}. \tag{4.14}$$

Lemma 4.2.3 *[3] Suppose $[H_t]_l \geq [S_t]_l$. One has*

$$\left|H - \widehat{S}\right| \leq \begin{cases} |H - S| - \frac{H_l - S_l}{N - S_l}|H_l - S_l| + 2\left[G(y, S_l) - H_l\right] & \text{if } y > y^u, \\ |H - S| - (1 - F(y, S_l))|H_l - S_l| & \text{if } y^u \geq y \geq S_l, \\ |H - S| + 2k|y - H_l| & \text{if } S_l > y. \end{cases}$$

In particular, when $y = H_l$, $|H - \widehat{S}| \leq |H - S| - (1 - F(y, S_l))|H_l - S_l|$.

PROOF.   Beginning with the middle case, $y \in [S_l, y^u]$, we note that the a posteriori strength at node l satisfies $\widehat{S}_l \in [S_l, H_l]$, i.e., where the observation noise is not as bad that the revised estimate could be worse than the a priori.

$$\Delta_l = \widehat{S}_l - S_l = G(y, S_l) - S_l = \frac{k(N - S_l)(y - S_l)}{N + k(y - S_l)}. \tag{4.15}$$

Due to the conservation of mass, the mass $\Delta_l > 0$ must be removed from the other nodes via $\widehat{S}_\lambda = F(y, S_l)S_\lambda$. In other words, these nodes will lose mass, that is $\widehat{S}_\lambda < S_\lambda$. The remaining nodes, $\mathcal{L} \setminus \{l\} = \mathcal{C}_1 \cup \mathcal{C}_2 \cup \mathcal{C}_3$, where $\mathcal{C}_1, \mathcal{C}_2, \mathcal{C}_3$ are disjoint, and given by

$$\mathcal{C}_1 = \{\lambda \in \mathcal{L} \setminus \{l\} | \widehat{S}_\lambda < S_\lambda < H_\lambda\},$$
$$\mathcal{C}_2 = \{\lambda \in \mathcal{L} \setminus \{l\} | H_\lambda \leq \widehat{S}_\lambda < S_\lambda\},$$
$$\mathcal{C}_3 = \{\lambda \in \mathcal{L} \setminus \{l\} | \widehat{S}_\lambda < H_\lambda \leq S_\lambda\}.$$

In the $\mathcal{C}_1$ case,

$$\begin{aligned} |H_\lambda - \widehat{S}_\lambda| = H_\lambda - \widehat{S}_\lambda &= H_\lambda - S_\lambda + S_\lambda - \widehat{S}_\lambda \\ &= (H_\lambda - S_\lambda) + (S_\lambda - \widehat{S}_\lambda) \\ &= |H_\lambda - S_\lambda| + S_\lambda(1 - F(y, S_l)). \end{aligned} \tag{4.16}$$

In the $\mathcal{C}_2$ case,

$$\begin{aligned} |H_\lambda - \widehat{S}_\lambda| = \widehat{S}_\lambda - H_\lambda &= S_\lambda - H_\lambda + \widehat{S}_\lambda - S_\lambda \\ &= |H_\lambda - S_\lambda| - (S_\lambda - \widehat{S}_\lambda) \\ &= |H_\lambda - S_\lambda| - S_\lambda(1 - F(y, S_l)). \end{aligned} \tag{4.17}$$

In the $\mathcal{C}_3$ case,

$$\begin{aligned} |H_\lambda - \widehat{S}_\lambda| = H_\lambda - \widehat{S}_\lambda &= H_\lambda - S_\lambda + S_\lambda - \widehat{S}_\lambda \\ &= (S_\lambda - \widehat{S}_\lambda) - (S_\lambda - H_\lambda) \\ &= S_\lambda(1 - F(y, S_l)) - (S_\lambda - H_\lambda). \end{aligned} \tag{4.18}$$

Lastly, we note that

$$\begin{aligned}
|H_l - \widehat{S}_l| &= H_l - \widehat{S}_l \\
&= H_l - \widehat{S}_l - S_l + S_l \\
&= H_l - S_l + (S_l - \widehat{S}_l) \\
&= |H_l - S_l| - \Delta_l.
\end{aligned} \tag{4.19}$$

Combining (4.16)–(4.19), one obtains,

$$|H - \widehat{S}| = \sum_{\lambda \in \mathcal{L}} |H_\lambda - \widehat{S}_\lambda| = \sum_{\lambda \in \mathcal{L} \backslash \mathcal{C}_3} |H_\lambda - S_\lambda| - \Delta_l + \sum_{\lambda \in \mathcal{C}_1 \cup \mathcal{C}_3} (S_\lambda - \widehat{S}_\lambda)$$
$$- \left\{ \sum_{\lambda \in \mathcal{C}_2} S_\lambda (1 - F(y, S_l)) + \sum_{\lambda \in \mathcal{C}_3} (S_\lambda - H_\lambda) \right\}.$$

By conservation of strength mass and by noting that $(S_\lambda - \widehat{S}_\lambda) > 0, \forall \lambda \in \mathcal{C}_2$, we have

$$\sum_{\lambda \in \mathcal{C}_1 \cup \mathcal{C}_3} (\widehat{S}_\lambda - S_\lambda) + \sum_{\lambda \in \mathcal{C}_2} (\widehat{S}_\lambda - S_\lambda) - \Delta_l = 0. \tag{4.20}$$

$$\sum_{\lambda \in \mathcal{C}_1 \cup \mathcal{C}_3} (\widehat{S}_\lambda - S_\lambda) - \Delta_l \leq 0. \tag{4.21}$$

Clearly, the inequality (4.21) holds true if one removes the middle term in equation (4.20). Therefore, combining (4.20) and (4.21), one has

$$|H - \widehat{S}| \leq \sum_{\lambda \in \mathcal{L} \backslash \mathcal{C}_3} |H_\lambda - S_\lambda| - \left\{ \sum_{\lambda \in \mathcal{C}_2} S_\lambda (1 - F(y, S_l)) + \sum_{\lambda \in \mathcal{C}_3} (S_\lambda - H_\lambda) \right\}$$

$$|H - \widehat{S}| \leq |H - S| - \left\{ \sum_{\lambda \in \mathcal{C}_2} S_\lambda (1 - F(y, S_l)) + \sum_{\lambda \in \mathcal{C}_3} (S_\lambda - H_\lambda) \right\}. \tag{4.22}$$

From there, we use the statement that

$$\sum_{\lambda \in \mathcal{C}_3} (S_\lambda - H_\lambda) \geq (1 - F(y, S_l)) \sum_{\lambda \in \mathcal{C}_3} (S_\lambda - H_\lambda). \tag{4.23}$$

In addition, we assume that

$$\sum_{\lambda \in \mathcal{C}_2} S_\lambda \geq \sum_{\lambda \in \mathcal{C}_2} (S_\lambda - H_\lambda). \tag{4.24}$$

By substituting (4.23) and (4.24) into (4.22), one obtains

$$|H - \widehat{S}| \leq |H - S| - \sum_{\lambda \in \mathcal{C}_2} (1 - F(y, S_l))(S_\lambda - H_\lambda)$$
$$- \sum_{\lambda \in \mathcal{C}_3} (1 - F(y, S_l))(S_\lambda - H_\lambda).$$

$$\leq |H - S| - \sum_{\lambda \in \mathcal{C}_2 \cup \mathcal{C}_3} (1 - F(y, S_l))(S_\lambda - H_\lambda). \tag{4.25}$$

Also, since $\sum_{\lambda \in \mathcal{L}}(S_\lambda - H_\lambda) = 0$, one has

$$\sum_{\lambda \in \mathcal{C}_2 \cup \mathcal{C}_3} (S_\lambda - H_\lambda) = (H_l - S_l) + \sum_{\lambda \in \mathcal{C}_1}(H_\lambda - S_\lambda) \geq H_l - S_l. \tag{4.26}$$

Thus, by substituting (4.26) into (4.25), one has

$$|H - \widehat{S}| \leq |H - S| - (1 - F(y, S_l))|H_l - S_l|, \tag{4.27}$$

which is the second case of the Lemma. Next, we look at the first case of the Lemma 4.2.3. This is the case where the a posteriori estimate, $\widehat{S}_l$, exceeds H_l. We add $\widehat{S}_l - S_l$ to the strength at node l. We remove this strength mass from all nodes $\mathcal{L} \setminus \{l\}$. We denote this added mass by the equation $\epsilon_l^u + (H_l - S_l) = \widehat{S}_l - S_l$. The additional mass, $H_l - S_l$, at l and removal of the same mass from $\mathcal{L} \setminus \{l\}$ provides the same estimate as given by case 2 where $y = y^u$. We, therefore, define the intermediary strength distribution to be $\widetilde{S}_t$ such that $[\widetilde{S}_t]_l = H_l$ and have

$$\widehat{S}_t - S_t = (\widehat{S}_t - \widetilde{S}_t) + (\widetilde{S}_t - S_t). \tag{4.28}$$

From case 2, we know that

$$|H - \widetilde{S}_t| \leq |H - S| - (1 - F(y^u, S_l))|H_l - S_l|. \tag{4.29}$$

By inserting y^u into $F(y, S_l)$, we have

$$F(y^u, S_l) = \frac{N - H_l}{N - S_l}. \tag{4.30}$$

Combining (4.29) and (4.30), we obtain

$$|H - \widetilde{S}_t| \leq |H - S| - \frac{H_l - S_l}{N - S_l}|H_l - S_l|. \tag{4.31}$$

From there, we wish to add excess mass, ϵ_l^u, at node l and remove it elsewhere. Since we are adding and removing ϵ_l^u, we must choose a worse-case bound such that

$$|\widehat{S}_t - \widetilde{S}_t| \leq 2\epsilon_l^u = 2[G(y, S_l) - H_l], \tag{4.32}$$

so that the inequality remains valid in the worst case. Combining (4.31) and (4.32), we obtain

$$|H - \widehat{S}_t| \leq |H - \widetilde{S}_t| + |\widehat{S}_t - \widetilde{S}_t|$$
$$\leq |H - S| - \frac{H_l - S_l}{N - S_l}|H_l - S_l| + 2[G(y, S_l) - H_l], \tag{4.33}$$

which proves the first case.

In the third case, we obtain an observation y that is less than S_l. We, therefore, have a negative effect where strength mass is removed from S_l due to the observation. Since $H_l > S_l > y$, we have

$$|\widehat{S} - H| = |\widehat{S}_l - H_l| + \sum_{\lambda \neq l} |S_\lambda - H_\lambda|. \tag{4.34}$$

Since $H_l > S_l > \widehat{S}_l$, we have

$$
\begin{aligned}
|\widehat{S} - H| &= H_l - \widehat{S}_l + \sum_{\lambda \neq l} |\widehat{S}_\lambda - H_\lambda| \\
&= (H_l - S_l) + (S_l - \widehat{S}_l) + \sum_{\lambda \neq l} |\widehat{S}_\lambda - S_\lambda + S_\lambda - H_\lambda| \\
&\leq (H_l - S_l) + (S_l - \widehat{S}_l) + \sum_{\lambda \neq l} |\widehat{S}_\lambda - S_\lambda| + \sum_{\lambda \neq l} |S_l - H_l| \\
&= |H - S| + |S_l - \widehat{S}_l| + \sum_{\lambda \neq l} |\widehat{S}_\lambda - S_\lambda| \tag{4.35}
\end{aligned}
$$

We know that $S_l > y$ and therefore $S_l > \widehat{S}_l$. That means also, $\widehat{S}_\lambda - S_\lambda > 0$. Therefore, we have

$$= |H - S| + (S_l - \widehat{S}_l) + \sum_{\lambda \neq l} (\widehat{S}_\lambda - S_\lambda) \tag{4.36}$$

We also know that $\sum_{\lambda \neq l} (\widehat{S}_\lambda - S_\lambda) = (S_l - \widehat{S}_l)$.

$$= |H - S| + 2(S_l - \widehat{S}_l) \tag{4.37}$$

$$= |H - S| + 2[S_l - G(y, S_l)] \tag{4.38}$$

The terms $[S_l - G(y, S_l)]$ simplifies to

$$
\begin{aligned}
S_l - G(y, S_l) &= S_l - \frac{S_l + k(y - S_l)}{1 + \frac{k(y - S_l)}{N}} \\
&= S_l \frac{1 + \frac{k(y - S_l)}{N}}{1 + \frac{k(y - S_l)}{N}} - \frac{S_l + k(y - S_l)}{1 + \frac{k(y - S_l)}{N}} \\
&= k(S_l - y) \frac{N - S_l}{N + k(y - S_l)} \\
&= \frac{kS_l(y - S_l) - kN(y - S_l)}{N + k(y - S_l)} \\
&= \frac{k(S_l - y)(N - S_l)}{N + k(y - S_l)} \tag{4.39}
\end{aligned}
$$

Since $y - S_l \geq -S_l$, we have $N + k(y - S_l) \geq N - kS_l$. If we substitute this inequality into the denominator of (4.39), we get

$$\leq k(S_l - y)\frac{N - S_l}{N - kS_l}$$

$$S_l - G(y, S_l) \leq k(S_l - y) \tag{4.40}$$

Combining (4.38) and (4.40) and knowing that $H_l > S_l > y$, we have

$$|H - \widehat{S}| \leq |H - S| + 2k(S_l - y)$$
$$\leq |H - S| + 2k(H_l - y)$$
$$= |H - S| + 2k|y - H_l|, \tag{4.41}$$

which proves the third case of the Lemma as well as completing the proof of Lemma 4.2.3.

Next, we will look at and prove the other case that is given by the following Lemma. Once again, we define $y^u = \overline{y}(H_l, S_l)$ where we evaluate $\widehat{S}_l$ with H_l in the equation from 4.12.

Lemma 4.2.4 *Suppose* $[H_t]_l \leq [S_t]_l$. *One has*

$$\left|\widehat{S} - H\right| \leq \begin{cases} |S - H| - \frac{S_l - H_l}{N - S_l}|S_l - H_l| + 2\left[H_l - G(y, S_l)\right] & \text{if } y < y^u, \\ |S - H| - (F(y, S_l) - 1)|S_l - H_l| & \text{if } y^u \leq y \leq S_l, \\ |S - H| + 2k|H_l - y| & \text{if } S_l < y. \end{cases}$$

PROOF.   Like the previous lemma, we begin with the middle case, $y \in [y^u, S_l]$. Also as before, note that this is the case where the a posteriori strength at node l satisfies $\widehat{S}_l \in [H_l, S_l]$, i.e., where the observation noise is not as bad that the revised estimate could be worse than the a priori. Unlike the previous lemma, however, the adjustment at the observed node is

$$\Delta_l = S_l - \widehat{S}_l = S_l - G(y, S_l) = \frac{k(S_l - N)(y - S_l)}{N + k(y - S_l)}. \tag{4.42}$$

Due to the conservation of mass, the mass $\Delta_l > 0$ must be added to the other nodes via $\widehat{S}_\lambda = F(y, S_l)S_\lambda$. In other words, these nodes will gain mass, that is $\widehat{S}_\lambda > S_\lambda$.

The remaining nodes, $\mathcal{L} \setminus \{l\} = \mathcal{C}_1 \cup \mathcal{C}_2 \cup \mathcal{C}_3$, where $\mathcal{C}_1, \mathcal{C}_2, \mathcal{C}_3$ are disjoint, and given by

$$\mathcal{C}_1 = \{\lambda \in \mathcal{L} \setminus \{l\} | S_\lambda < \widehat{S}_\lambda < H_\lambda\},$$
$$\mathcal{C}_2 = \{\lambda \in \mathcal{L} \setminus \{l\} | H_\lambda \le S_\lambda \le \widehat{S}_\lambda\},$$
$$\mathcal{C}_3 = \{\lambda \in \mathcal{L} \setminus \{l\} | S_\lambda < H_\lambda \le \widehat{S}_\lambda\}.$$

In the $\mathcal{C}_1$ case,

$$
\begin{aligned}
|\widehat{S}_\lambda - H_\lambda| &= H_\lambda - \widehat{S}_\lambda = H_\lambda - S_\lambda + S_\lambda - \widehat{S}_\lambda \\
&= (H_\lambda - S_\lambda) - (\widehat{S}_\lambda - S_\lambda) \\
&= |S_\lambda - H_\lambda| - S_\lambda(F(y, S_l) - 1).
\end{aligned}
\tag{4.43}
$$

In the $\mathcal{C}_2$ case,

$$
\begin{aligned}
|\widehat{S}_\lambda - H_\lambda| &= \widehat{S}_\lambda - H_\lambda = \widehat{S}_\lambda - S_\lambda + S_\lambda - H_\lambda \\
&= (\widehat{S}_\lambda - S_\lambda) + S_\lambda - H_\lambda \\
&= S_\lambda(F(y, S_l) - 1) + |S_\lambda - H_\lambda|.
\end{aligned}
\tag{4.44}
$$

In the $\mathcal{C}_3$ case,

$$
\begin{aligned}
|\widehat{S}_\lambda - H_\lambda| &= \widehat{S}_\lambda - H_\lambda = \widehat{S}_\lambda - S_\lambda + S_\lambda - H_\lambda \\
&= (\widehat{S}_\lambda - S_\lambda) + S_\lambda - H_\lambda \\
&= S_\lambda(F(y, S_l) - 1) - (S_\lambda - H_\lambda).
\end{aligned}
\tag{4.45}
$$

Lastly, as before, we note that

$$
\begin{aligned}
|\widehat{S}_l - H_l| &= \widehat{S}_l - H_l \\
&= \widehat{S}_l - H_l + S_l - S_l \\
&= S_l - H_l + (\widehat{S}_l - S_l) \\
&= |S_l - H_l| - \Delta_l.
\end{aligned}
\tag{4.46}
$$

Combining (4.43)–(4.46), one obtains,

$$
|\widehat{S} - H| = \sum_{\lambda \in \mathcal{L}} |\widehat{S}_\lambda - H_\lambda| = \sum_{\lambda \in \mathcal{L} \setminus \mathcal{C}_3} |S_\lambda - H_\lambda| - \Delta_l + \sum_{\lambda \in \mathcal{C}_2 \cup \mathcal{C}_3} (\widehat{S}_\lambda - S_\lambda) \tag{4.47}
$$
$$
- \left\{ \sum_{\lambda \in \mathcal{C}_1} S_\lambda(F(y, S_l) - 1) + \sum_{\lambda \in \mathcal{C}_3} (H_\lambda - S_\lambda) \right\}.
$$

Using the principle of conservation of strength mass and the case that $(\widehat{S}_\lambda - S_\lambda) > 0, \forall \lambda \in \mathcal{C}_1$, we state that

$$\sum_{\lambda \in \mathcal{C}_2 \cup \mathcal{C}_3} (\widehat{S}_\lambda - S_\lambda) + \sum_{\lambda \in \mathcal{C}_1} (\widehat{S}_\lambda - S_\lambda) - \Delta_l = 0. \tag{4.48}$$

$$\sum_{\lambda \in \mathcal{C}_2 \cup \mathcal{C}_3} (\widehat{S}_\lambda - S_\lambda) - \Delta_l \leq 0. \tag{4.49}$$

Clearly, the inequality (4.49) must hold true if one removes the middle term in equation (4.48). Therefore, combining (4.47) and (4.49), one has

$$|\widehat{S} - H| \leq \sum_{\lambda \in \mathcal{L} \setminus \mathcal{C}_3} |S_\lambda - H_\lambda| - \left\{ \sum_{\lambda \in \mathcal{C}_1} S_\lambda(F(y, S_l) - 1) + \sum_{\lambda \in \mathcal{C}_3} (H_\lambda - S_\lambda) \right\}$$

$$|\widehat{S} - H| \leq |S - H| - \left\{ \sum_{\lambda \in \mathcal{C}_1} S_\lambda(F(y, S_l) - 1) + \sum_{\lambda \in \mathcal{C}_3} (H_\lambda - S_\lambda) \right\}. \tag{4.50}$$

From there, we use the statement that

$$\sum_{\lambda \in \mathcal{C}_3} (H_\lambda - S_\lambda) \geq (F(y, S_l) - 1) \sum_{\lambda \in \mathcal{C}_3} (H_\lambda - S_\lambda) \text{ if } F(y, S_l) \leq 2. \tag{4.51}$$

We examine the condition that $F(y, S_l) \leq 2$ through the definition of $F(y, S_l)$.

$$F(y, S_l) = \frac{1}{1 + k\frac{y - S_l}{N}} \leq 2 \tag{4.52}$$

With some algebraic manipulation we have

$$1 + k\frac{y - S_l}{N} \geq \frac{1}{2}$$

$$(S_l - \frac{N}{2k}) \leq y \tag{4.53}$$

Thus, we set the constraint such that y (the right side of 4.53) must be greater than or equal to the difference of the left side expression in order for (4.52) to hold true. In addition, we assume that

$$\sum_{\lambda \in \mathcal{C}_1} S_\lambda \geq \sum_{\lambda \in \mathcal{C}_1} (H_\lambda - S_\lambda), \text{ which is true if } 2S_\lambda > H_\lambda > S_\lambda. \tag{4.54}$$

By substituting (4.51) and (4.54) into (4.50), one obtains

$$|\widehat{S} - H| \leq |S - H| - \sum_{\lambda \in \mathcal{C}_1} (F(y, S_l) - 1)(H_\lambda - S_\lambda)$$

$$- \sum_{\lambda \in \mathcal{C}_3} (F(y, S_l) - 1)(H_\lambda - S_\lambda).$$

$$\leq |S - H| - (F(y, S_l) - 1) \sum_{\lambda \in \mathcal{C}_1 \cup \mathcal{C}_3} (H_\lambda - S_\lambda). \tag{4.55}$$

Also, since $\sum_{\lambda \in \mathcal{L}} (H_\lambda - S_\lambda) = 0$, one has

$$\sum_{\lambda \in \mathcal{C}_1 \cup \mathcal{C}_3} (H_\lambda - S_\lambda) = (S_l - H_l) + \sum_{\lambda \in \mathcal{C}_2} (S_\lambda - H_\lambda) \geq S_l - H_l. \tag{4.56}$$

Thus, by substituting (4.56) into (4.55), one has

$$|\widehat{S} - H| \leq |S - H| - (F(y, S_l) - 1)|S_l - H_l|, \tag{4.57}$$

which is the second case of the Lemma. We now take a look at the first case of the Lemma. This is the case where the observation noise y is less compared to y^u that the a posteriori estimate, $\widehat{S}_l$, ends up being less than H_l, that is $\widehat{S}_l < H_l$. We remove $S_l - \widehat{S}_l$ from the strength at node l. We add this mass to nodes $\mathcal{L} \setminus \{l\}$. We denote the adjustment mass, $S_l - \widehat{S}_l$, by the equation $\epsilon_l^u + (S_l - H_l) = S_l - \widehat{S}_l$. The removal of the strength mass $S_l - H_l$ at l and the addition of mass at $\mathcal{L} \setminus \{l\}$ gives the same estimate as the second case where $y = y^u$. Let this intermediary strength distribution be $\widetilde{S}_t$ where $[\widetilde{S}_t]_l = H_l$ and we have

$$S_t - \widehat{S}_t = (S_t - \widetilde{S}_t) + (\widetilde{S}_t - \widehat{S}_t) \tag{4.58}$$

From the second case, we have the inequality

$$|\widetilde{S}_t - H| \leq |S - H| - (F(y^u, S_l) - 1)|S_l - H_l| \tag{4.59}$$

In order for the middle case to hold true for also the first case, we must bound y^u so that $F(y^u, S_l)$ evaluates to some number between one and two. Therefore, we have

$$1 < F(y^u, S_l) \leq 2 \tag{4.60}$$

$$1 < \frac{1}{1 + k\frac{(y^u - S_l)}{N}} \leq 2$$

$$1 > 1 + k\frac{(y^u - S_l)}{N} \geq \frac{1}{2}$$

$$0 > k\frac{(y^u - S_l)}{N} \geq -\frac{1}{2}$$

$$0 > (y^u - S_l) \geq -\frac{N}{2k}$$

$$S_l > y^u \geq S_l - \frac{N}{2k}$$

$$S_l - \frac{N}{2k} \leq y^u < S_l. \tag{4.61}$$

From the previous Lemma, we defined $y^u = \bar{y}(H_l, S_l)$, which evaluates to

$$y^u = \frac{N(H_l - S_l) + kS_l(N - H_l)}{k(N - H_l)} \tag{4.62}$$

Using this definition, we evaluate $F(y^u, S_l)$ as

$$F(y^u, S_l) = \frac{1}{1 + k\left[\dfrac{\frac{N(H_l - S_l) + kS_l(N - H_l)}{k(N - H_l)} - \frac{kS_l(N - H_l)}{k(N - H_l)}}{N}\right]}$$

$$= \frac{N - H_l}{N - S_l}. \tag{4.63}$$

By substituting the evaluated expression from (4.63) into (4.59), we have

$$|\widetilde{S}_t - H| \leq |S - H| - \frac{S_l - H_l}{N - H_l}|S_l - H_l| \tag{4.64}$$

The other adjustment composed of $\widetilde{S}_t - \widehat{S}$ requires removing ϵ_l^u at node l and adding it elsewhere. For the worst case, we apply a worst-case bound such that

$$|\widetilde{S}_t - \widehat{S}| \leq 2\epsilon_l^u = 2[H_l - G(y, S_l)] \tag{4.65}$$

Finally, by combining (4.64) and (4.65), we obtain

$$|\widehat{S}_t - H| \leq |\widetilde{S}_t - H| + |\widetilde{S}_t - \widehat{S}_t|$$

$$\leq |S - H| - \frac{S_l - H_l}{N - H_l}|S_l - H_l| + 2[H_l - G(y, S_l)]. \tag{4.66}$$

For the third case, we have an observation y that is greater than our estimate, S_l. Therefore, we obtain a posteriori estimate that is greater than the truth H_l. Using the fact that $y > S_l > H_l$, we state that

$$|\widehat{S} - H| = |\widehat{S}_l - H_l| + \sum_{\lambda \neq l}|\widehat{S}_\lambda - H_\lambda| \tag{4.67}$$

$$= (\widehat{S}_l - S_l) + (S_l - H_l) + \sum_{\lambda \neq l}|\widehat{S}_\lambda - S_\lambda + S_\lambda - H_\lambda|$$

$$\leq |S_l - H_l| + |\widehat{S}_l - S_l| + \sum_{\lambda \neq l}|\widehat{S}_\lambda - S_\lambda| + \sum_{\lambda \neq l}|\widehat{S}_\lambda - H_\lambda|$$

$$\leq |S - H| + |\widehat{S}_l - S_l| + \sum_{\lambda \neq l}|\widehat{S}_\lambda - S_\lambda|. \tag{4.68}$$

By conservation of strength, we say that $\sum_{\lambda \neq l}(S_\lambda - \widehat{S}_\lambda) = \widehat{S}_l - S_l$. Therefore, the right hand side of inequality (4.68) can be rewritten as

$$= |S - H| + 2(\widehat{S}_l - S_l) \tag{4.69}$$

$$= |S - H| + 2[G(y, S_l) - S_l]$$

$$= |S - H| + 2\left[\frac{S_l + k(y - S_l)}{1 + k\frac{y - S_l}{N}} - \frac{S_l(1 + k\frac{y - S_l}{N})}{1 + k\frac{y - S_l}{N}}\right]$$

$$= |S - H| + \frac{kN(y - S_l) - kS_l(y - S_l)}{N + k(y - S_l)}$$

$$= |S - H| + \frac{k(N - S_l)(y - S_l)}{N + k(y - S_l)}. \tag{4.70}$$

Taking the second term of the inequality in (4.70) and using the fact that $S_l < y$, we claim

$$\frac{N - S_l}{N + k(y - S_l)} < 1 \tag{4.71}$$

$$N - S_l < N + k(y - S_l).$$

We can therefore substitute the right hand side of inequality (4.71) into (4.70). And finally, using the case $S_l > H_l$, we arrive at the final case where

$$|\widehat{S} - H| \leq |S - H| + 2k(y - S_l) \tag{4.72}$$

$$|\widehat{S} - H| \leq |S - H| + 2k(y - H_l) \tag{4.73}$$

$$|\widehat{S} - H| \leq |S - H| + 2k|H_l - y|, \tag{4.74}$$

thus completing the proof of the Lemma.

4.3   Simulation Example: Expected True Strength versus Estimated Strength

Since we compare the difference between the expected true strength and estimated strength, we will include all 500 locations within the set $l \in \mathcal{L}$. We choose to have a single Red team in which we simulate the probable location of its movement at five time-steps. In our plot for the expect true strength, the color coding in the larger area depicts the terrain type of the location, i.e., water bodies, building corners, etc. The Red team starts at the same location at the beginning of the simulation regardless of

whether we have a commander input. We designate the Red team at the initial location with a true strength of $H_l = 3$, which is denoted by the red circles in the right plot of the simulation. The probable flow of the Red units occurs by following the Markov chain property of the flow matrices, $\mathcal{F}$ or $[\mathcal{F} + U_t]$, when we have a commander input in our simulation. For the nominal flow of the Red units, we will set the diagonal entry(ies), $\eta_{nom} = \mathcal{F}_{i,i} = 0.7$, and the rest of the strength mass being evenly distributed through the connected edges of the graph. If we have a commander input at a particular time-step, the diagonal entry(ies) will be modified such that, $\eta_{com} = [\mathcal{F} + U_t]_{i,i} = 0.3$, with the rest of the strength mass being evenly distributed through the connected edges of the graph. To understand how we define the two matrices, we provide an example below at a particular time-step:

$$\mathcal{F} = \begin{pmatrix} 0.7 & 0.1 & 0.1 & \dots & 0.1 \\ 0.3 & 0.7 & 0 & \dots & 0 \\ 0 & 0.15 & 0.7 & \dots & 0.15 \\ \dots\dots\dots\dots\dots\dots\dots\dots\dots \\ 0 & 0.15 & 0.15 & \dots & 0.7 \end{pmatrix}, \; U_t = \begin{pmatrix} -0.4 & 0.13 & 0.13 & \dots & 0.13 \\ 0 & 0 & 0 & \dots & 0 \\ 0 & 0 & 0 & \dots & 0 \\ \dots\dots\dots\dots\dots\dots\dots\dots\dots \\ 0 & 0.2 & 0.2 & \dots & -0.4 \end{pmatrix} \tag{4.75}$$

$$\mathcal{F} + U_t = \begin{pmatrix} 0.3 & 0.23 & 0.23 & \dots & 0.23 \\ 0.3 & 0.7 & 0 & \dots & 0 \\ 0 & 0.15 & 0.7 & \dots & 0.15 \\ \dots\dots\dots\dots\dots\dots\dots\dots\dots \\ 0 & 0.35 & 0.35 & \dots & 0.3 \end{pmatrix}. \tag{4.76}$$

We see from the corresponding rows in Matrix 4.76 that we have a commander input in at least the first and L^{th} location. The probability flow for the Red units will be much greater at those locations at that time-step. We see in the above example that even though we introduce a commander input, the basic Markov property still upholds. That is, $\sum_{j\in\mathcal{L}}[\mathcal{F}]_{i,j} + [U_t]_{i,j} = 1 \quad \forall\, i \in \mathcal{L}$.

In this simulation, we introduce the input parameter c, where c is the probability that a commander input occurring per time-step. To understand the extent to which the Red commander input (analogous to a disturbance in our system) affects our final estimate assessment, we set $c = 0.5$.

We obtain the expected true strength distribution, $\mathbf{E}[H_t]$, using Monte Carlo simulations with $I = 1000$ iterations at five time-steps. We obtain this distribution using

both nominal flow matrix, $\mathcal{F}$, and the commander input matrix, $[\mathcal{F} + U_t]$ when we have a commander input. Specifically, at each iteration at each time-step, suppose we were to have a random variable, r, be some number such that $0 < r < 1$. Since we know that $\sum_{j \in \mathcal{L}} \mathcal{F}_{i,j} = 1, \forall i \in \mathcal{L}$, and $\sum_{j \in \mathcal{L}} [\mathcal{F}]_{i,j} + [U_t]_{i,j} = 1, \forall i \in \mathcal{L}$, we would determine at what matrix row indices does our r value lie in between. For example, suppose in our ground truth distribution, the true strength is initially located at node 1. Suppose the connected locations to node 1 are nodes 5, 10, and 15. Therefore, in our nominal flow matrix, our entries for the first row would be $\mathcal{F}_{1,1} = 0.7$, $\mathcal{F}_{1,5} = 0.1$, $\mathcal{F}_{1,10} = 0.1$, and $\mathcal{F}_{1,15} = 0.1$. If our random variable $r = 0.85$, then $[\mathcal{F}_{1,1} + \mathcal{F}_{1,5}] < r < [\mathcal{F}_{1,1} + \mathcal{F}_{1,5} + \mathcal{F}_{1,10}]$. As a result, for the Red units, the new location at the next time-step would be at node 10. We would repeat this procedure at each time-step for each iteration and record the new positions of the Red units. Then, we compute the expected true strength distribution by taking the mean true strength of the iterations for each time-step.

In our expected true strength plot, whenever we have a commander input in our simulation, we will denote the distribution for the nominal flow and the commander input flow (actual flow) as cyan circles and red circles, respectively. When we only have nominal flow at a particular time-step, the circles will be represented by the color green.

In implementing observation in our simulation, we will parameterize the probability of an observation at a particular location with p_l. We denote p_l to be some number from 0 to 1. In our simulation results, we evaluate $p_l = 0.5$.

For the estimated strength distribution, we assume that we are given complete information of the Red team's strength and location at the first time-step. We obtain the estimated strength distribution at the next time-steps using Monte Carlo simulations with $I = 1000$ iterations where each time-step involves a dynamic flow update followed by an observation update. The final distribution of the estimated strength will depend upon how we evaluate the flow parameter, η_{nom}, and the observation parameter, p_l.

We assume that our observations are corrupted by random noise; we will have imperfect observations of the Red units within the terrain. We include this random noise into our simulation by first creating a normal distribution for the possible observation measurements, $[y_t]_l$. We take the mean, μ_y, to be the true strength, H_l. We parameterize the standard deviation, σ_y, for the noise, to be some value such that $0 < \sigma_y \leq 1$. Using the normal distribution function given by equation 4.77, we determine the probability bounds corresponding to our possible observation measurements with which a random

variable r between 0 and 1 lies:

$$p = F(y|\mu_y, \sigma_y) = \frac{1}{\sigma_y \sqrt{2\pi}} \int_{-\infty}^{y} e^{\frac{-(t-\mu_y)^2}{2\sigma_y^2}} dt \qquad (4.77)$$

Once we determine the probability bound with which our random variable r lies, we select the corresponding observation bin and take the rounded value to be the observation strength, $[y_t]_l$. We will, for this example, take $\sigma_y = 1$ in order to analyze fully the effects of noise on the final estimated strength distribution.

Suppose, for example, we take the ground truth to be the mean, $\mu_y = H_l = 3$, and the observation noise to be $\sigma_y = 1$. That means that, for our normal distribution (See Figure 4.1), we will have seven bins along the interval $[0,6]$, which represent our observation potential measurements.
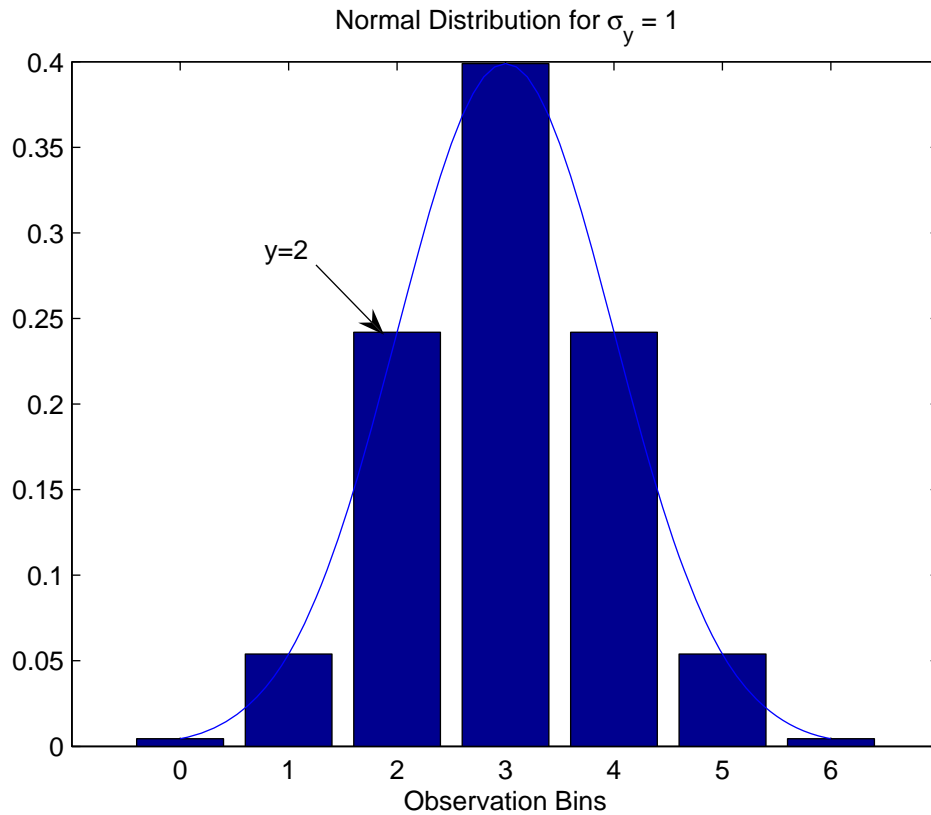

Figure 4.1: Example with Observation Noise, $\sigma_y = 1$, $\mu_y = 3$

Suppose now that $r = 0.35$, then our random variable would lie within the area of our normal distribution curve that corresponds to Observation Bin 2 since the probability interval is approximately $(0.16, 0.5]$. Therefore, in this instance, our observation

measurement is $[y_t]_l = 2$. It is also worth noting that one standard deviation to either the left or right of our mean, $\mu_y = 3$, composes of a large area under our probability curve (68.2%), revealing that we most often will have our observation measurements, $[y_t]_l = 2$ or 3 or 4.

Once our simulation illustrates favorable results, we compute the error bound for the dynamic flow and the observation disturbance effects.

4.4   Simulation Results

In the plots below, we simulated the results of our estimated strength distribution and the expected true strength distribution given the conditions that we discussed in the Section 4.3. We test to see how well our estimator distribution compares with the expected true strength when we place observation noise and commander inputs in our model. These can also be viewed as disturbances and measurement noises in the system. In the end, our estimator must converge to the expected true strength.
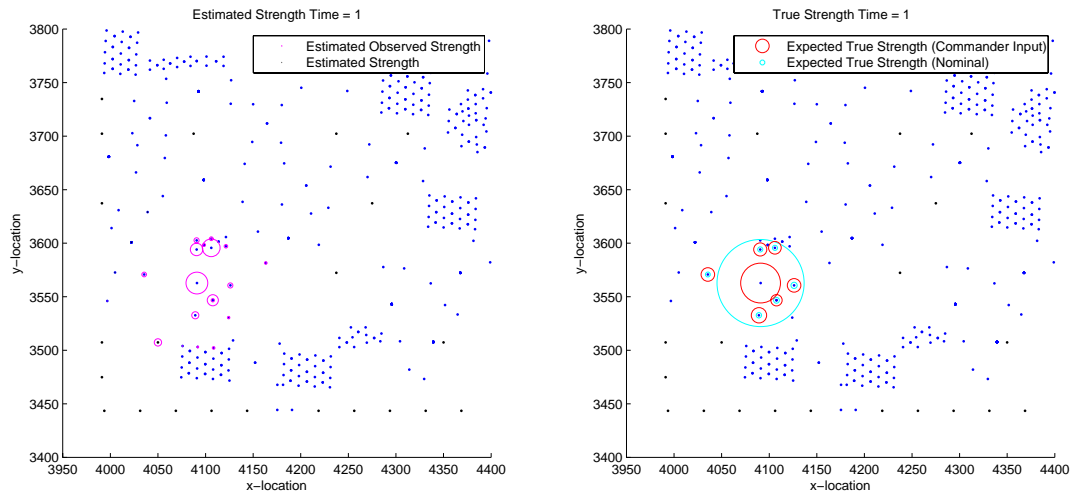

Figure 4.2: Stochastic Flow, Initial Time-Step

At the initial time-step of our simulation, the right-half plot in Figure 4.2 indicates that we have a commander input where the red circles indicate the actual flow (with the commander input), and the cyan circles indicate the nominal flow if no input occurred for that time-step. We see that the actual flow for the simulation ($\eta_{com} = 0.3$) has the strength mass diffusing rapidly from the initial location of the true

strength compared to the nominal flow ($\eta_{nom} = 0.7$) where most of the strength mass is concentrated at the initial location. We see from the actual flow that most of the strength mass has been evenly distributed to the connected edges of the graph.

For the estimated strength plot (left plot in Figure 4.2), we obtain similar trends from the expected true strength plot but with a different analysis. Based on our algorithm, we know that the strength estimator has no memory of the commander input and therefore is computed nominally. However, we must also take into consideration the observation factor. Besides where the ground truth is located, at a particular iteration and time-step, we may have observations (random noise) at connected nodes. In our plot, besides the original location, we see that throughout all 1000 iterations, most of the connected locations had an observation (as indicated by the magenta circles). This indicates that the observation update holds the mass closer to the location being observed no matter if we have observation due to random noise.
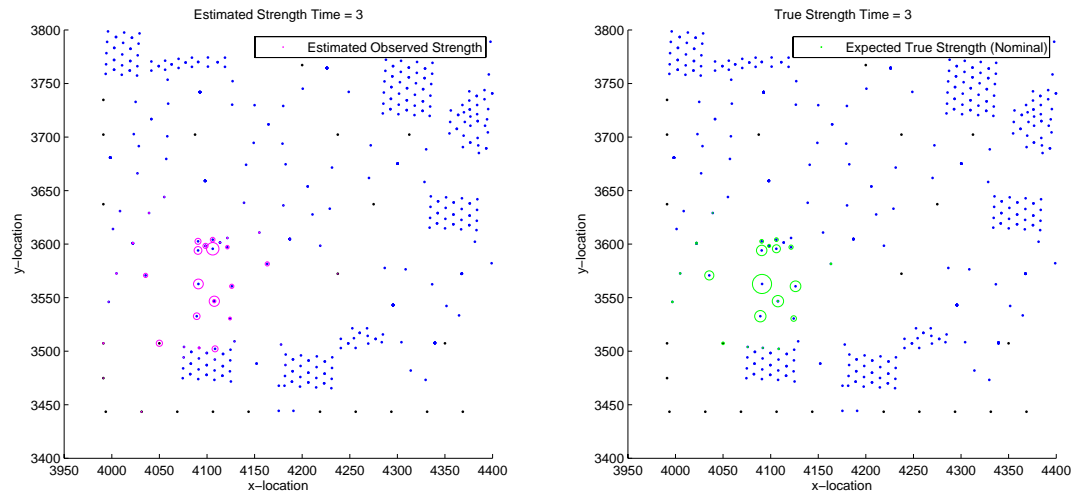

Figure 4.3: Stochastic Flow, Time-Step 3

In Figure 4.3 at time-step 3, we have only nominal flow in our true strength plot as represented by the green circles. As a result, we have more strength mass being concentrated at the original location(s) since $\eta_{nom} = 0.7$.

For the strength estimator plot, we see that largely all of the circles are magenta. This indicates that out of 1000 iterations, we are bound to have an observation update at every location connected to the original starting point. Note that our estimator distribution, although we have several observational locations looks somewhat different

from the expected ground truth. We must consider the fact that our observation noise parameter is $\sigma_y = 1$. Therefore, our observations will not be as accurate ($y = H_l$). As a result, our estimate may not be as close to the ground truth we would like.
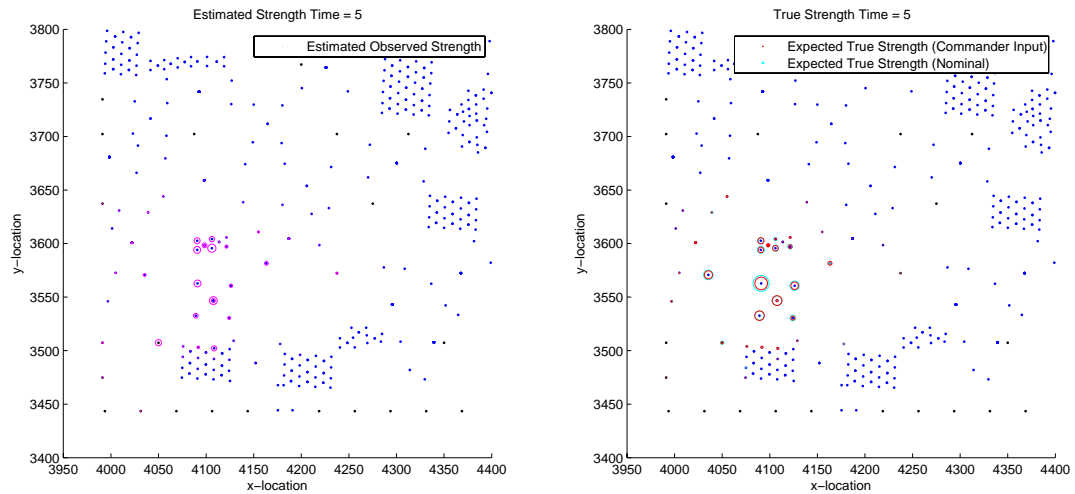

Figure 4.4: Stochastic Flow, Final Time-Step

In Figure 4.4, we see an indication from our expected true strength plot of a commander input signal, and therefore we see an even wider flow of red circles. If we compare that to the nominal flow, we notice that some of the red circles and the cyan circles are approximately the same size. The red circles are somewhat smaller. We can therefore conclude that given enough time, the strength distribution will diffuse across regardless of how high our flow parameters are.

For the estimator plot, we see, interestingly, a wider spread in our distribution. In some locations/waypoints, we have more strength mass than what we had at our original location. Also, if we compare this plot with our expected true strength plot, we apparently have more mass at some locations and less others, suggesting that we both underestimate and overestimate our measurements. This indicates that the observation update plays a significant role in the final distribution for our estimator.

4.4.1 Analysis: Dynamics Effects

In Table 4.1, we computed the left side and right side of the inequality in Theorem 4.2.2. As with the deterministic case, the same can be said of the error bounds for this case. We notice that for the left side of the inequality in this simulation, the error

Table 4.1: Dynamic Error Bounds

Time-steps	Left Side	Right Side
1	2.2126	2.2126
2	1.8378	4.6126
3	1.7305	7.8459
4	1.7394	7.8459
5	1.5154	7.8459

bound is reduced, which would indicate that over time, our estimate, S_t, will improve ($S_t \approx \mathbf{E}[H_t]$). This is particularly true since $\mathbf{E}[H_t]$ should converge to S_t. If we analyze the right side of our error bound inequality, we see that the commander input occurs only twice in our simulation. Moreover, suppose we run this simulation for more than five time-steps. We can claim that the more commander inputs we have, the larger our error bounds for the right side of Theorem 4.2.2 will be.

4.4.2 Analysis: Observation Disturbance Effects

Table 4.2: Observation Disturbance Effects Error Bounds

Time-steps	Left Side	Right Side
1	3.6220	5.7952
2	5.4951	7.4948
3	6.3256	8.1765
4	6.7283	8.5228
5	7.0405	8.7713

In Table 4.2, we computed the error bound for the observation by applying Lemma 4.2.3 in the case where $[H_t]_l \geq [S_t]_l$ and applying Lemma 4.2.4 in the case where $[H_t]_l \leq [S_t]_l$. Setting the number of iterations equal to 1000, we did this by applying the **L1** norm to the left and right side of the two inequalities where appropriate for each sub-case.

From the data in our table, we can see that the left side of the inequality gradually increases at each time-step. Since we know that the **L1** norm allows us to compare our a posteriori estimator, $\widehat{S}$, with our ground truth, H_t, we can see that our observation error becomes worse as time passes. One possible reason for this is that over time, we have a much greater variation of our estimated strength distribution due to the observation noise in our measurements. As a result, our a posteriori estimator, $\widehat{S}$, may

become far from the ground truth as the time-steps increase even though we may have some good observations $(y = H_l)$.

Table 4.3: Detailed Error Bounds

	$[H_t]_l \geq [S_t]_l$			$[H_t]_l \leq [S_t]_l$		
Time-steps	$y > y^u$	$y^u \geq y \geq S_l$	$S_l > y$	$y < y^u$	$y^u \leq y \leq S_l$	$S_l < y$
1	808	394	1970	298	79	451
2	294	1639	1399	354	58	266
3	245	2007	1192	301	47	208
4	240	2137	1083	304	50	186
5	223	2207	1028	300	47	195
Total	1800	8384	6672	1557	281	1306

According to Table 4.3, when we verified that both Lemmas hold true, we found on the right side of the inequality that the sub-case where $y^u \geq y \geq S_l$ appeared the most often in the overall iteration process. In fact, in the table, we see that over the five time-steps, the sub-case appeared 8384 times. We would consider this to be a positive finding since it would indicate that the observation, y, made at each iteration is within range of the ground truth. However, at the very first time-step, it appears the least in the first Lemma. The reason is that both the estimate, S_l, and the ground truth, H_l, begin at the same location. That is, $S_l = H_l$. Since the $y^u = H_l$ when $S_l = H_l$, the only possible situation where the middle sub-case applies is $y = S_l = y^u$. The chance that this sub-case appears in our computation has significantly been diminished.

However, when Lemma 4.2.4 was applied to the computation, the middle sub-case occurred least often. Based on the condition that $y^u \leq y \leq S_l$, we see that despite the fact that the estimator, S_l was greater the truth, H_l, our observation, y, was still within range of the truth itself $(y \leq H_l)$. That is, our observation underestimates the truth more often but does not overestimate very much.

5

Estimation Behavior Analysis

Using the stochastic case, we analyze the results at each time-step of the strength estimator,$[S_t]_l$, and compare them to the simulated true strength data, $[H_t]_l$. We investigate how the final results of the estimator will differ by varying the different results of the input parameters.

5.1 Statistical Computation

In our analysis, we relate the estimated strength, $[S_t]_l$, with the true strength, $[H_t]_l$, by computing the mean bias error, $\overline{e_t}$ and the mean standard deviation, $\overline{\sigma_t}$ of our data and see how they vary with the input parameters that we control. Using several iterations, we must first compute expected bias error, $e_{t,l}$, and the standard deviation, $\sigma_{t,l}$, which we obtain by the following equations:

$$e_{t,l} = \frac{1}{I} \sum_{i=1}^{I} ([\widehat{S}_t]_l{}^i - [H_t]_l{}^i) \tag{5.1}$$

$$\sigma_{t,l} = \sqrt{\frac{1}{I-1} \sum_{i=1}^{I} [([\widehat{S}_t]_l{}^i - [H_t]_l{}^i) - e_{t,l}]^2}. \tag{5.2}$$

When we compute the standard deviation, we subtract the error, $e_{t,l}$, in our computation in order to get a more accurate measure in our standard deviation.

We, from there, compute the mean bias error and mean standard deviation by

taking the average of (5.1) and (5.2) across all 500 locations:

$$\overline{e_t} = \frac{1}{L} \sum_{l=1}^{L} e_{t,l} \tag{5.3}$$

$$\overline{\sigma_t} = \frac{1}{L} \sum_{l=1}^{L} \sigma_{t,l}. \tag{5.4}$$

5.2   Comparing the Results for the Estimator and the True Strength

5.2.1   Effects of Observation Confidence and Observation Noise

We vary our initial parameters to see how it affects the final outcome in our data. We choose to keep our observation parameter, p_l, constant ($p_l = 1$). Therefore, at each iteration, we will always have an observation occurring. We will keep the dynamic flow update parameter the same ($\eta_{nom} = 0.7$ and $\eta_{com} = 0.3$). In Subsection 5.2.1, we vary the k value and the observation noise, σ_y, in our simulations in order to see to what degree they will affect the results of our data. We measure these effects by computing the mean bias error (5.3) and the mean standard deviation (5.4). In Subsection 5.2.1, we develop a better understanding as to what degree the input parameter will cause the estimator to deviate from the true data.

In Figure 5.1, we varied our k value and observation noise to obtain surface plots of the mean error at the final time-step. We notice that varying the parameters has very little effect on the outcome of the mean error. We see this from the various fluctuations across the graph of the error, suggesting that we do not see much of a relationship between the two input parameters. It is though worth mentioning that our error itself is indeed infinitesimally small (by a factor of 10^{-18}) that the difference between our estimator and the ground truth is negligible. Therefore, we have an unbiased error in our estimator.

The interesting aspect of the error plot is that our bias error becomes large when $k \geq 1$ and $\sigma_y \approx 0$. We know that in this instance $y = H_l = 0$ or $y < S_l$. When this occurs, we must be mindful of our choice for k. If we choose the wrong k value, we will have an error division by zero in the computation for the a posteriori estimate, $\widehat{S_l}$, and our plot will show the error diverge to infinity. We see this indication that we may approach such a value. Let us analyze the restriction for k. We analyze the denominator
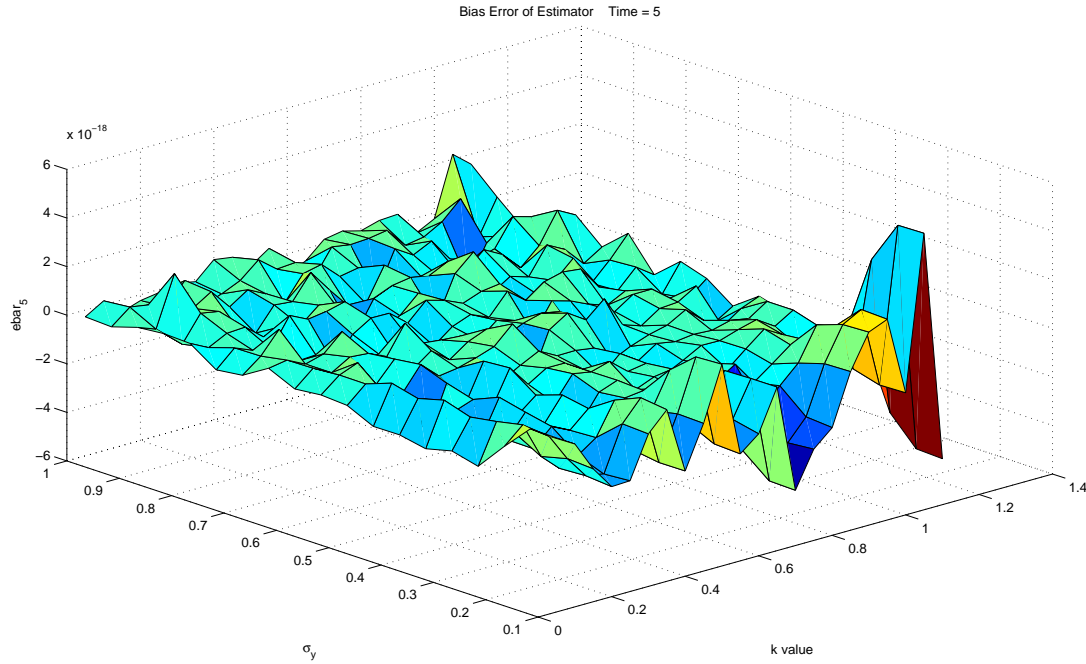
Figure 5.1: Mean Bias Error versus (Observation Confidence, Observation Noise), Final Time-Step

of our observation update, $\widehat{S}_l$:

$$1 + k\frac{y - S_l}{N} \neq 0$$

Algebraically manipulating the inequality above, we obtain the following restriction for k:

$$k \neq \frac{N}{S_l - y}, \tag{5.5}$$

where $S_l > y$.

Also, unlike the mean error, in Figure 5.2, we see a significant correlation between the input parameters themselves and our output, the mean standard deviation. We see, on one hand, when our k value is large and our observation is large, our mean standard deviation will be large. However, if we reduce our observation noise, σ_y, we reduce the mean standard deviation substantially. This relation suggests that a high k value with a low observation noise input value will provide us with a more accurate estimate of the actual ground truth. We know this to be true since the k parameter tells us the level of confidence we have in our actual observation of the Red units while the observation noise reveals how perfect our observation would be. In addition, if we choose a low k value, we are suggesting that we have very little confidence in our observation
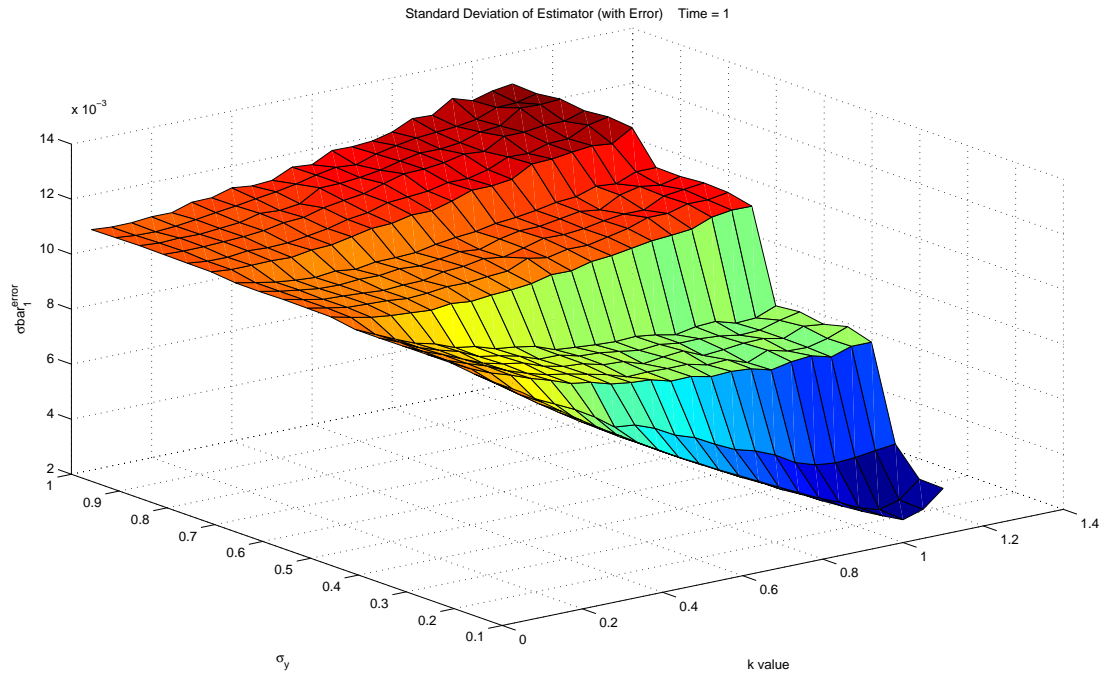
Figure 5.2: Mean Standard Deviation versus (Observation Confidence, Observation Noise), Initial Time-Step

and therefore our observation noise, σ_y, becomes irrelevant to our estimate itself. In other words, not only does our estimate depend on k but also the degree to which the observation noise influences our estimate depends on k as well. Therefore, if we have perfect observation (no errors) of the adversary and we are confident in our method, we will obtain a more accurate estimate of the ground truth itself as revealed by the mean standard deviation in the figure.

Also, we notice that the observation noise is reduced in discrete steps downward. In our algorithm, we implemented our observation measurements, y, such that any observation noise in our measurements is represented by the standard deviation of a normal distribution. If we have a measurement that is not a natural number, we must round that value since we will see only distinct Red units in the terrain itself. As a result, varying the precision by a small factor in the observation noise will not make a significant difference in the outcome of the mean standard deviation since our rounded y will still be the same.

The plot in Figure 5.3 follows the same trend as our plot in the initial time-step. Essentially, as before, our mean standard deviation for our estimator and true strength
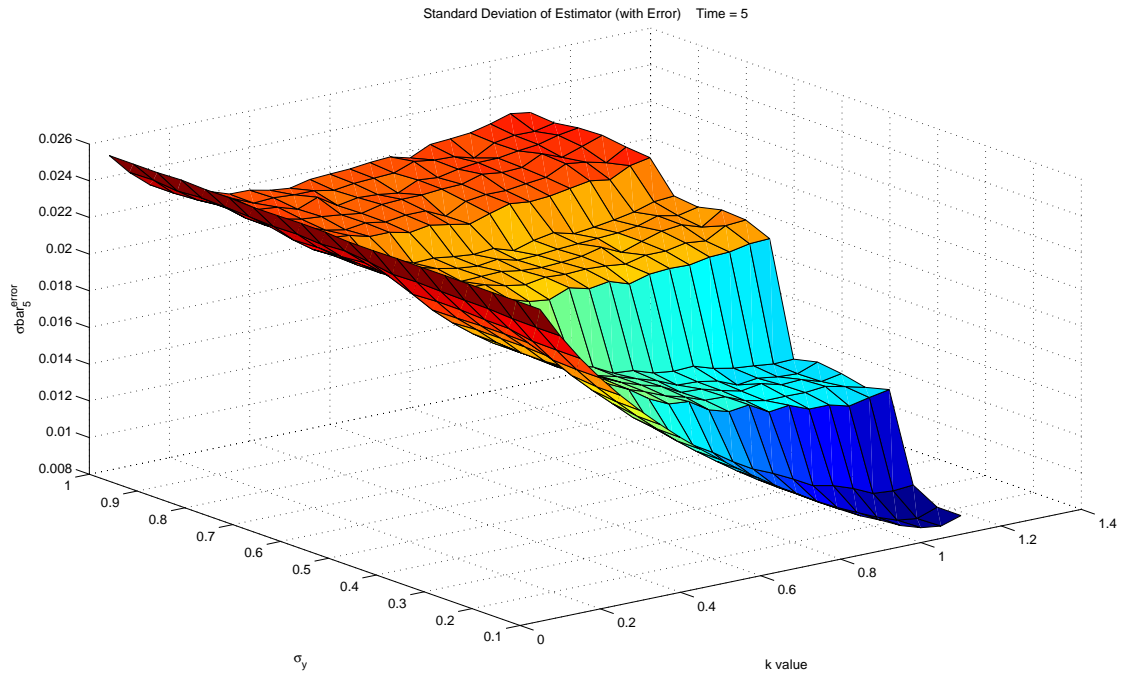
Figure 5.3: Mean Standard Deviation versus (Observation Confidence, Observation Noise), Final Time-Step

diminishes as we increase k and decrease σ_y in discrete steps. The difference, though, is that our standard deviation becomes large much faster when we increase the observation noise. We know that the more close σ_y is to one, the more imperfect our observation of the Red units will be. Thus, if we continue to make observations that are poor at each and every time-step, then we will certainly have an estimate that is far from the truth itself as illustrated by the larger standard deviation.

In addition, as we increase σ_y, we note that the mean standard deviation does not decrease as much when we increase k. From the surface plot in Figure 5.3, when σ_y is large our standard deviation stays approximately the same regardless of the k value, suggesting that the observation update makes no difference in the final estimate. Let us therefore analyze this further.

We optimize our k value as we vary our observation noise such that we choose the k value that minimizes the mean standard deviation, $\overline{\sigma_t}$. In Figure 5.4, we vary the precision by 0.01 of the observation noise as opposed to the surface plot (precision by 0.05) in order to determine specifically where the standard deviation is minimized. In the plot, we note that our optimal value fluctuates more as our observation noise variation
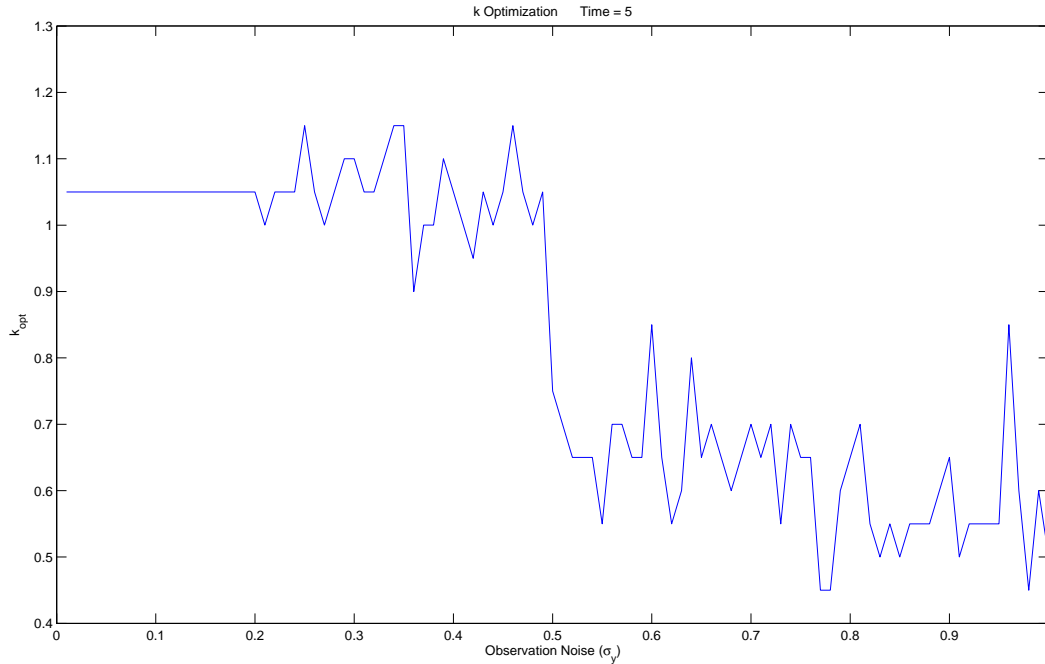
Figure 5.4: k Value Optimization, Final Time-Step

becomes more precise. Even if this is the case, we still gain a better understanding with regards to our k_{opt} value when the noise is small and when it is large. We see in Figure 5.4 that for the final time-step, the k_{opt} is approximately greater than one when the observation noise is small. In fact, if we take the average of the k values such that $0.1 \leq \sigma_y \leq 0.5$, then we have $k_{opt} = 1.05$ as the average. For all k values such that $0.5 \leq \sigma_y \leq 1$, we have $k_{opt} = 0.6176$ as the average. Clearly, if we increase the noise, then k must be reduced since the observation measurements, y, will not be as accurate $(y = H_l)$ as often.

5.2.2 Effects of Flow Parameter and Commander Input

In the following analysis, we will vary the input parameters for the dynamic flow update to look at their relationship to the mean standard deviation of our strength estimator and the true strength. Since we would like to look only at the effects that the flow update has on our estimator, we will keep observation update parameters constant. For this computation, we set the remaining parameters to the following values: $k = 0.95$, $\sigma_y = 1$, and $p_l = 1$.

In Figure 5.5, we vary the dynamic flow update parameters, η_{nom} and η_{com},
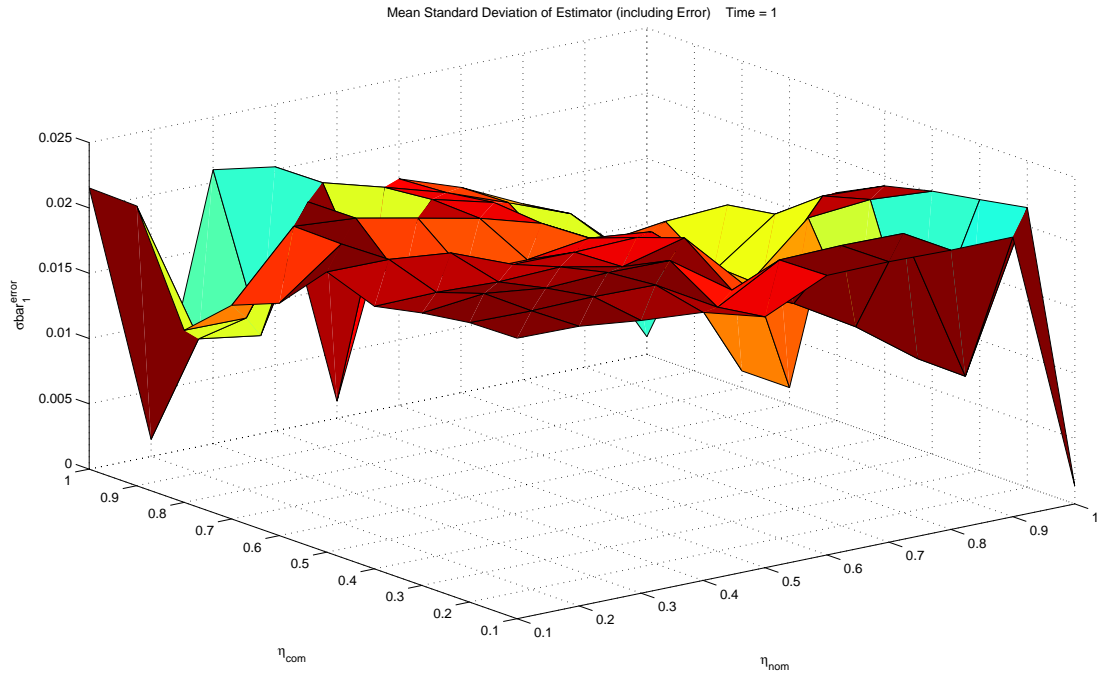
Figure 5.5: Mean Standard Deviation versus (Commander Input, Nominal Flow), Initial Time-Step

to analyze the effects on the mean standard deviation. We see that, at the first time-step, the standard deviation does not fluctuate as much when the two parameters are low. We know that when we choose small flow parameter values to run our simulation, our estimator distribution would spread more thinly across the board. Therefore, for a particular time-step, our standard deviation will remain at its extrema when we choose smaller parameter values. On the other hand, as we increase η_{com} and η_{nom}, we see that the standard deviation varies more.

In Figure 5.6, we see after a few time-steps that for the large flow parameter values, the mean standard deviation converges to the same value corresponding to the lowest flow parameter value. In addition, we notice that the converged standard deviation value has also shifted up, suggesting that over time we may have high number of locations with non-negligible strength.

At the last time-step in Figure 5.7, we have less kinks than we had initially. We can see much clearly that for large parameter values, the mean standard deviation converges much closely to the standard deviation for when our flow parameters are small. This would imply that over time the strength distribution will diffuse to a more uniform
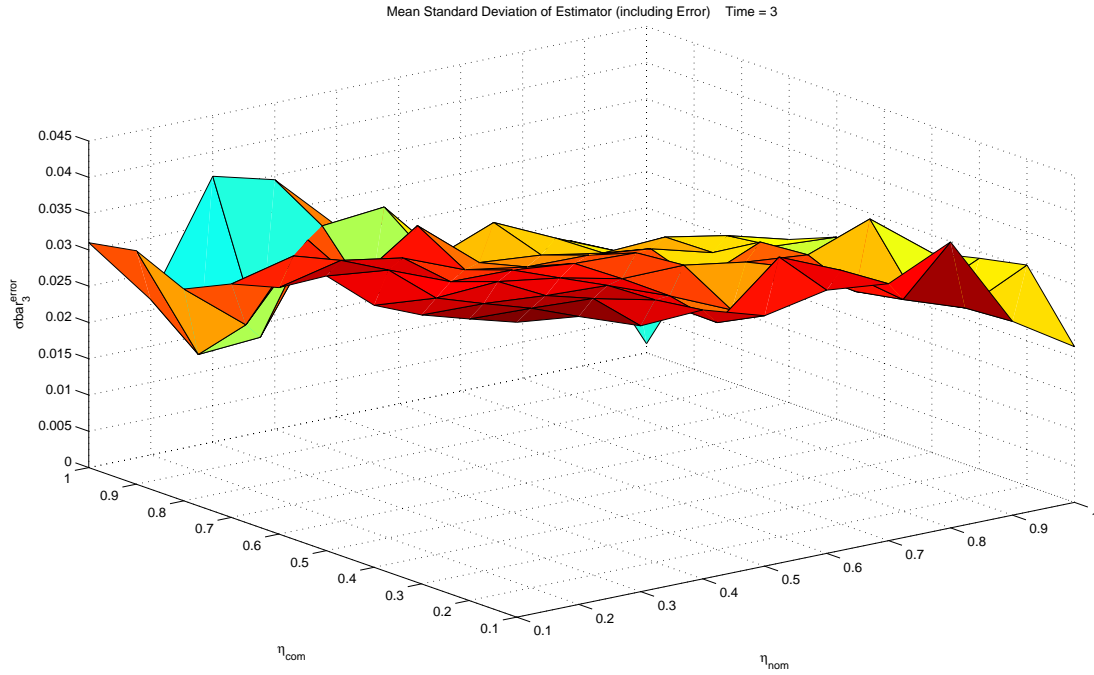
Figure 5.6: Mean Standard Deviation versus (Commander Input, Nominal Flow), Time-Step 3

distribution. Therefore, given enough time-steps, our choice for the flow update parameters would become irrelevant to the final outcome of the estimated strength distribution.

5.2.3 Effects of Observation Probability and Observation Noise

We will vary the probability of observation per location (p_l). We will vary this with the observation noise itself, based on the direct relationship between the two. All other parameters are kept the same. We set the other parameter values equal to the following: $k = 0.95, \eta_{nom} = 0.7, \eta_{com} = 0.3$.

Similar to Figures 5.2 and 5.3, we see that the mean standard deviation is reduced when we decrease our observation noise, σ_y, and, this time, when we increase our probability of observation, p_l. We realize that observing the actual true strength, H_l, of the Red units itself will improve our estimate, S_t. That is, the more observations taking place will improve our estimate substantially. In addition, we must ensure that our observation is perfect. Therefore, decreasing the observation noise will provide us with a better estimate as represented by the mean standard deviation plot given above in Figure 5.8.
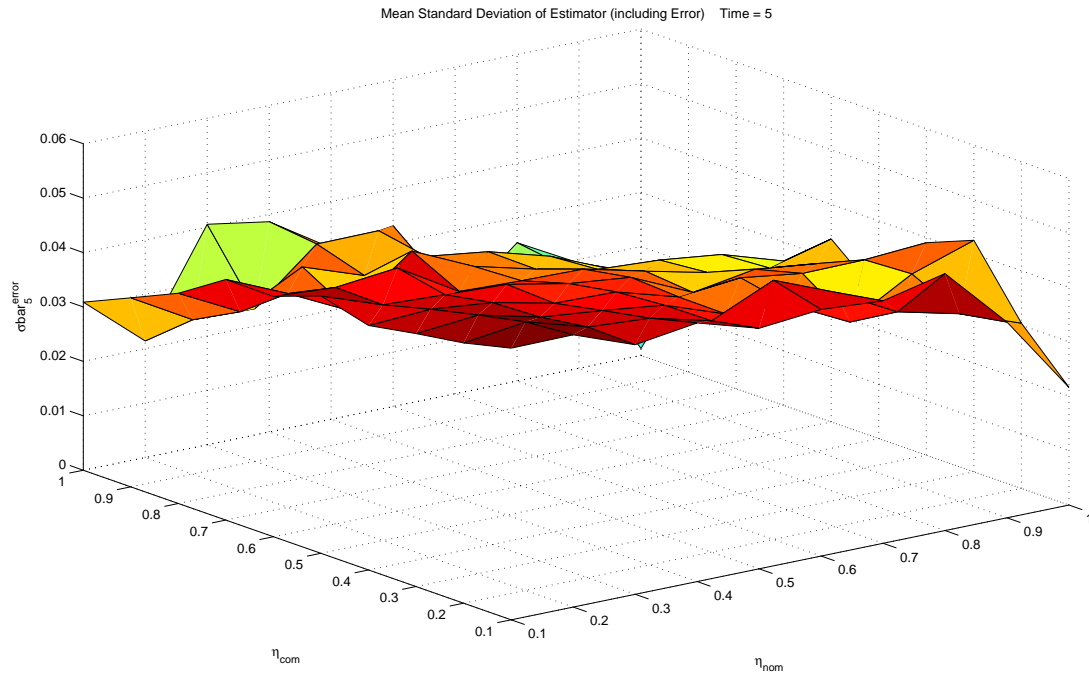
Figure 5.7: Mean Standard Deviation versus (Commander Input, Nominal Flow), Final Time-Step

The plot in Figure 5.9 follows the same trend as the plot in Figure 5.8. As we increase the time-steps, the mean standard deviation has shifted up more. Let us analyze the extreme cases of the parameters. We notice that when our observation probability is close to one and the noise is close to zero, our mean standard deviation is minimized like our initial time-step. However, the standard deviation is reduced even further than from the initial time-step for the same parameter values. We can see that the more perfect observation that we have over each time-step will provide us with a best estimate in the end. Suppose instead that probability of observation is large but our observation noise is large as well. Hence, we have a highly imperfect observation method. We can conclude that despite all our observations over time, our estimate, S_l, will be far from the truth, H_l as represented by the large standard deviation. Finally, it is clearly evident that our observation noise, σ_y, becomes irrelevant if our probability of observation parameter, p_l, is small.
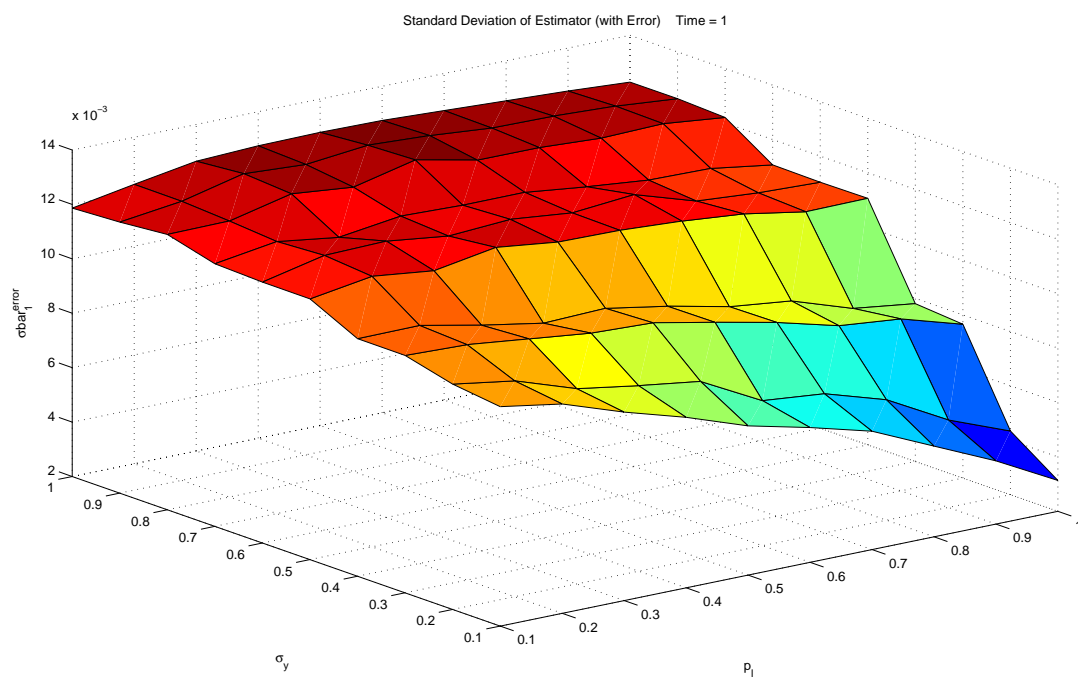
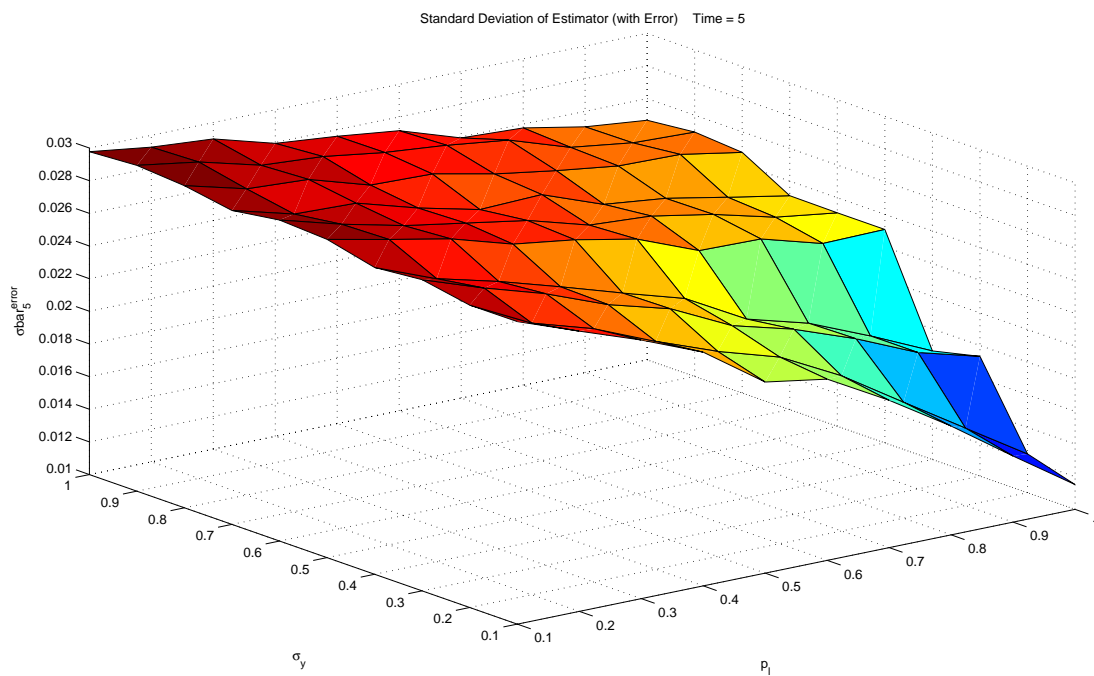Figure 5.8: Mean Standard Deviation versus (Observation Probability, Observation Noise), Initial Time-Step

Figure 5.9: Mean Standard Deviation versus (Observation Probability, Observation Noise), Final Time-Step

6

Conclusions

In this thesis, we sought to objectively model the force distribution (manpower) of an adversary within a set terrain and compared it to the ground truth–a subjective topic in nature. Through simulations and numerical computations, we determined how well our adversarial estimator reflects the ground truth using the stochastic methods presented. We explored two cases where our methods were implemented: natural deterministic flow and primarily the stochastic flow. Our simulation results have shown that for the stochastic case, our strength estimator converges quite well to our generated expected true strength.

For the stochastic case, we assumed we had limited knowledge of the state of the ground truth itself such as location, strength, and the probable movements of the Red units. In our simulation, the probable movement of the Red units at each time-step was represented by either a nominal flow transition matrix or commander input matrix, where the input is analogous to disturbance in the system. Seeing that the state of the system may change as a result of this disturbance, we applied a Bayesian observation update in order to adjust our strength estimator so that it may better reflect the true strength itself.

Once we obtained our stochastic estimator using the arbitrary input parameters selected, our job was to optimize those parameters in order to produce an estimate that minimizes the standard deviation between our estimated strength and the true strength. For instance, we developed a better understanding with regards our various observation parameters such as the k value and the observation noise, σ_y. We are able to optimize our k value depending on the noise in our system. The observation noise, analogous to a

measurement noise in a system, depends upon how clearly and confidently we view the adversary. Through this type of analysis, we learned that the input parameters, which represent our general understanding of the battlefield and the adversary, can determine how close our assessment is to reality.

6.1 Future Work

As the research in this topic comes to an end, we have another area that we yet to have touched. Our analysis in adversarial estimation can become more complex when we introduce attrition into our model. Attrition is the gradual reduction of strength in numbers or size. In our case, the reduction would be in manpower of the Red units, assume we have multiple fire teams. From the observation measurements made, our job is to produce a decent estimate of the adversary, while, at the same time, considering attrition occuring in our ground truth.

We must therefore determine an algorithm for our simulation that will display the attrition in our system. Some of the suggested means to show this is computing the expectation of the true strength, using probabilities of reduction in strength from the size of manpower. We may find the need to be more subjective in modeling this. For example, we may believe that a single unit Red fire team would have high chance of vulnerability then a multiple unit fire team.

Another method that we may choose to consider is fuzzy logic[5]. Some of the variables that determine attrition is the observation measurements and the distance between the Blue and Red teams. We may choose to establish some rules with regards to the distance (i.e.,close, near, far) and observation measurements (i.e. $y = 1$, $y = 2$, $y = 3$, etc.), which we use to determine our output: the level of reduction of the Red forces (ΔH_l). Once again, we seek to apply a systematic method to model a subjective topic. Thus, in determining the best method, we must consider many factors.

Bibliography

[1] W. M. McEneaney and R. Singh. A computationally-feasible algorithm for estimation of opponent strength in urban combat. *Proc. 12t Intl. Command and Control Res. and Tech. Symposium, Newport*, (2007).

[2] W. M. McEneaney and R. Singh. A low-complexity observer for urban combat reconnaissance applications. *Preprint*, (2007).

[3] W. M. McEneaney, R. Singh, and D. Panchal. An estimator for processing uav-reconnaissance data in support of run operations. *AIAA Guidance, Nav. and Control Conf.*, (2007).

[4] J. Norris. *Markov Chains*. Cambridge University Press, 1998.

[5] R. Zhang. *Fuzzy Control of Queuing Systems*. Springer-Verlag London Limited, 2005.